

Original Article

Characterization of ligamentum flavum hypertrophy based on m6A RNA methylation modification and the immune microenvironment

Zhongyuan He^{1,2*}, Zhengya Zhu^{1*}, Tao Tang^{1,2*}, Peng Guo^{1,2}, Manman Gao^{3,4}, Baoliang Li^{1,2}, Tran Canh Tung Nguyen⁵, Hongkun Chen¹, Xizhe Liu², Zhiyu Zhou¹, Shaoyu Liu^{1,2}

¹Innovation Platform of Regeneration and Repair of Spinal Cord and Nerve Injury, Department of Orthopaedic Surgery, The Seventh Affiliated Hospital, Sun Yat-sen University, Shenzhen, Guangdong, China; ²Guangdong Provincial Key Laboratory of Orthopedics and Traumatology, The First Affiliated Hospital of Sun Yat-sen University, Guangzhou, Guangdong, China; ³Department of Sport Medicine, Inst Translat Med, The First Affiliated Hospital of Shenzhen University, Shenzhen Second People's Hospital, Shenzhen, Guangdong, China; ⁴Guangdong Key Laboratory for Biomedical Measurements and Ultrasound Imaging, School of Biomedical Engineering, Shenzhen University Health Science Center, Shenzhen, Guangdong, China; ⁵Department of Orthopaedic Surgery, Faculty of Medicine, University of Toyama, Toyama, Japan. *Co-first authors.

Received July 12, 2022; Accepted November 29, 2022; Epub December 15, 2022; Published December 30, 2022

Abstract: Objective: N6-methyladenosine (m6A) has been implicated in the progression of several diseases, and the role of epigenetic regulation in immunity is emerging, particularly for RNA m6A modification. However, it is unclear how m6A-related genes affect the immune microenvironment of ligamentum flavum hyperplasia (LFH). Therefore, we aimed to investigate the effect of m6A modification on the LFH immune microenvironment. Methods: The GSE113212 dataset was downloaded from the Gene Expression Omnibus (GEO) database. We systematically analyzed m6A regulators in eight patient samples and the corresponding clinical information of the samples. Gene Ontology (GO), Kyoto Encyclopedia of Genes and Genomes (KEGG), Gene Set Enrichment Analysis (GSEA) and protein-protein interactions (PPIs) were used to explore the correlation of m6A clusters with the immune microenvironment in LFH. A least absolute shrinkage and selection operator (Lasso) regression was then used to further explore the m6A prognostic signature in LFH. The relative abundance of immune cell types was quantified using a single-sample Gene Set Enrichment Analysis (ssGSEA) algorithm. We explored the relationship between hub genes and small molecule drug sensitivity by clustering hub gene-based samples. In addition, Real-Time quantitative PCR (RT-qPCR) as well as western blotting (WB) were used to validate the gene expression of the differentially expressed genes. Results: A total of 1259 differentially expressed genes were identified, of which 471 were upregulated and 788 were downregulated. A total of three genes showed significant differences (METTL16, PCIF1, and FTO). According to the enrichment analysis, immune factors may play a key role in LFH. ssGSEA was used to cluster the immune infiltration score, construct the hub gene diagnosis model, and screen a total of 6 LFH immune-related prediction model genes. The predictive diagnostic model of LFH was further constructed, revealing that METTL16, PCIF1, FTO and ALKBH5 had superior diagnostic efficiency. RT-qPCR results showed that 6 genes (METTL16, PCIF1, POSTN, TNNC1, MMP1 and ACTA1; $P < 0.05$) exhibited expression consistent with the results of the bioinformatics analysis of the mRNA microarray. Up-regulated METTL16, PCIF1, and ALKBH5 levels in LFH were validated by western blotting. Conclusion: Diversity and complexity of LFH's immune microenvironment are influenced by M6A modification, and our study provides strong evidence for predicting the diagnosis and prognosis of LFH.

Keywords: Ligamentum flavum hypertrophy, immune microenvironment, m6A RNA methylation, epigenetics, diagnostic model

Introduction

The occurrence of spinal stenosis is associated with multiple factors, of which lesions in the

ligamentum flavum (LF) account for a large proportion [1-3]. Clinically, hypertrophy of the ligamentum flavum (LFH) and ossification of the ligamentum flavum (OLF) are the main patho-

Ligamentum flavum hypertrophy on m6A and immune microenvironment

logical types. Hypertrophy of the ligamentum flavum is an early lesion is characterized by increased thickness, a decreased elastin collagen ratio, cartilage metaplasia, and advanced fibroblast ossification that aggravates local calcification, potentially leading to spinal stenosis and severe myelopathy [4-6].

Apart from decompressive surgery, no effective prevention and treatment options are available. Inflammation, macrophage infiltration, and fibrosis are key factors in this pathological process. A number of mechanical and biochemical factors have been identified as contributing to the development of LFH, as well as multiple molecules involved in the pathology [7-10]. Although aging, mechanical stress, inflammatory factors, transforming growth factor- β 1 (TGF- β 1), cyclooxygenase-2, tissue inhibitor of matrix metalloproteinases, and MMPs are thought to be involved in the hypertrophy of LF, the pathogenesis of LFH remains unclear [11-13].

A variety of human diseases are closely associated with aberrant m6A methylation modification according to recent studies. N6-methyladenosine (M6A) regulators have generated dramatic differences in the modification, gene expression, alternative splicing, and protein translation of noncoding RNAs, including long noncoding RNAs, microRNAs, and circular RNAs. These include RNA splicing, translocation, stability, and protein translation. METTL3, METTL14, ZC3H13, WTAP, RBM15B, and RBM15 are the core members of M6A, which is a multicomponent methyltransferase complex. Its regulators comprise three types of factors: writers (mainly METTL3-14, WTAP, HAKAI, WTAP and KIAA1429), readers (YTHDC1, YTHDC2, IGF2BP2, IGF2BP3, YTHDF1/2/3, HNRNPA2-B1, HNRNPC, and RBMX), and erasers (ALKBH5 and FTO). M6A mutations and abnormal expression lead to aberrant processes, including misregulation of cell death and proliferation, developmental defects, and impaired self-renewal [14-16]. M6A regulation can explain some of the underlying mechanisms of immune regulation. The microenvironment includes histiocytes, stromal cells, and recruited cells at distant sites, such as infiltrating immune cells (myeloid and lymphoid cells), bone marrow-derived cells (BMDCs) [17], and secreted factors, such as cytokines and chemokines, and

their interaction plays a crucial role in disease progression. For example, upon DNA viral infection, HNRNPA2B1 recognizes viral DNA and promotes m6A modification, triggering the innate immune response. In addition, m6A also plays an important role in adaptive immunity [18]. There is a paucity of literature investigating the relationship between RNA methylation modifications and LFH. In-depth study of the immune alterations between healthy samples and LFH samples as well as the changes in m6A regulators between these alterations will deepen the understanding of LFH pathogenesis from a completely new perspective. Fortunately, public databases provide transcriptome data related to LFH, whereas the use of RNAseq and RNAseq is becoming cheaper and more widespread, helping us to perform an integrated analysis of m6A RNA methylation.

The gene expression Omnibus database (GEO) was retrieved for data in this study, and expression levels of m6A-related genes were compared between LFH samples and normal ligamentum flavum tissues to examine the role of these genes in the immune microenvironment and LFH progression. We also clustered LFH samples according to nine m6A regulators and identified three different m6A modification patterns, LFH infiltrating immune cell abundance and immune responses. Gene sets were significantly associated with m6A regulators, suggesting that m6A regulators are closely related to immune regulators. The above results indicate that the m6A modification pattern has a significant impact on the immune microenvironment of LFH patients. These results provide new insights into the utilization of bioinformatics tools for the diagnosis and treatment of LFH.

Material and methods

Data preprocessing

The LFH disease chip data with data number GSE113212 <https://www.ncbi.nlm.nih.gov/geo/query/acc.cgi?acc=GSE113212> and clinical data of human samples were obtained from the GEO database and the GPL17077 sequencing platform [19]. The GSE113212 dataset contained a total of 8 patients, including 4 normal samples and 4 patients with LFH. The R package SVA [20] was used to correct for

Ligamentum flavum hypertrophy on m6A and immune microenvironment

batch effects present between different datasets and to perform log₂ normalization, and the expression distribution before and after normalization as well as after batch correction was visualized using box plots.

Expression values were normalized using the “normalize between arrays” function of the “limma” package in R software to obtain a similar distribution of expression values across the two groups [21]. Differential analysis of groupings was performed using the R package limma based on the grouping information in the data. Genes with logFC > 1 and *p*-value < 0.05 were considered upregulated genes, and genes with logFC < -1 and *P* value < 0.05 were considered downregulated genes.

Functional and pathway enrichment analysis of differentially expressed genes in nonhypertrophic specimens and LFH samples

Gene Ontology (GO) functional annotation analysis is a common method for conducting large-scale functional enrichment studies of genes and includes biological process (BP), molecular function (MF), and cellular components (CC). The Kyoto Encyclopedia of Genes and Genomes (KEGG) is a widely used database that stores information about genomes, biological pathways, diseases, and drugs. ClusterProfiler was used to analyze GO functional annotations and KEGG pathway enrichment analyses of differentially expressed genes associated with ligamentum flavum hypertrophy [22], and a *P* value < 0.05 was considered statistically significant in this study.

Assessment of immune heterogeneity across different m6A modification patterns

This study employed Gene Set Enrichment Analysis (GSEA) to analyze the distribution tendency of genes that are part of a predefined gene set ranked according to the extent of their correlation with the phenotype, and thus to evaluate the contribution of these genes to the phenotype [23]. We subjected the datasets to GSEA by taking the “c2.kegg.V7.4.Symbols” gene set in the MsigDB database using the “clusterprofiler” R package, and a false discovery rate (FDR) < 0.25 and |NES| > 1 was considered statistically significant [24]. This method of enrichment analysis assesses the variation in pathway activity of a simple population

unsupervised using gene set variation analysis (GSVA). Through the transformation of gene expression quantity matrix across samples into a pathway activation score matrix, the GSVA quantifies the gene enrichment results, making subsequent statistical analyses more convenient by evaluating whether metabolic pathways are enriched across different samples. In order to identify gene sets with significant differences between samples, a differential analysis of the GSVA results can be performed using the limma package. We obtained “msigdb.V7.0.symbols.gmt” and the gene set of phenotypic features from the MSigDB database to perform GSVA analysis on the dataset using the “GSVA” R package [25]. The R package “limma” was used to perform comparisons between the normal and LFH groups, and an adj *P* value < 0.01 was considered statistically significant.

Protein-protein interaction (PPI) network analysis and protein drug interaction analysis

In a protein-protein interaction network, individual proteins interact with one another to participate in a variety of biological processes, including signal transmission, gene expression regulation, cellular metabolism, and energy metabolism. For a comprehensive understanding of how proteins function, how biological signals work, the metabolism of energy substances in special physiological states, and the functional links between proteins, a systematic analysis of the interactions of protein in biological systems is necessary.

Among the 2031 species in the STRING database, a database of known and predicted protein-protein interactions, there are 9.6 million proteins and 138 million interactions between them [26]. It contains results obtained through experimental data, results derived from text mining PubMed abstracts and synthesis of other database data, as well as results predicted using bioinformatics techniques. We constructed a PPI network using the STRING database for the differentially expressed genes that were immunologically associated with ligamentum flavum hypertrophy, and this network was visualized using Cytoscape software. To identify the key modules and genes of the PPI network, cluster analysis using Molecular Complex Detection (MCODE) of Cytoscape was conducted. Genes that were immunologically associat-

Ligamentum flavum hypertrophy on m6A and immune microenvironment

ed with hypertrophy of the ligamentum flavum in modules with scores > 10 were considered to be the most differentially expressed genes.

We further targeted the hub genes for protein drug interaction analysis. Protein and drug target information was collected from the DrugBank database (version 5.0) [15] only for the portion of human data. The DrugBank database has also been significantly improved in terms of its content, interface, and performance, which has greatly improved its ease of use, utility, and potential applications in many areas, such as pharmaceutical science, pharmacology research, and pharmaceutical education.

Correlation analysis between m6A regulators and immune characteristics

Various cytokines and chemokines are present in the inflammatory microenvironment, including immune cells, fibroblasts, and stromal tissue. It is a load integrated system. Immune cell infiltration plays an influential role in disease research, treatment, and prognosis prediction. The R package ssGSEA was used to further evaluate the similarities and differences between the two groups in terms of immune cell infiltration levels. The background gene set for the ssGSEA was prepared by obtaining the marker genes of 28 immune cells from the literature [27].

To maximize the accuracy of the findings, the infiltration level of immune cells was assessed using an alternative method, the R package CIBERSORT [28], which calculates the content of 22 immune cells per sample based on the LM22 background gene set provided by CIBERSORT and thus reflects the infiltration level. The results were presented as heatmaps and stacked bar graphs, which were drawn using the R package ggplot2. Similarly, a scatter plot of correlations was plotted and fitted to the correlation curve for gene immune cell pairs for which the correlation was significant.

Diagnostic model constructed based on the m6A gene

Considering the importance of m6A modification, normal and patient samples may have different m6A modification statuses. Therefore, a diagnostic model based on m6A-related genes

is feasible. Here, we first screened all m6A genes using the Lasso regression method, which was implemented using the R package “glmnet” and selected the optimal lambda value. Regression was only performed on genes with coefficients not equal to 0, and the genes used to construct the model and their corresponding coefficients were visualized as forest plots using the R package “forestplot”.

Subsequently, to reveal the common influence of the m6A gene with other clinical features, such as age and sex, on the diagnostic efficacy of the model, the most significantly weighted genes as well as age and sex information from the previous Lasso model were constructed using the R package “rms” and visualized using a nomogram. To validate the predictive efficacy of the diagnostic model, single-gene Receiver operating characteristic (ROC) curves were drawn, and the area under the curve was calculated using the R package “pROC”. To illustrate the validity of the nomogram, in-house datasets and DCA curves were used for validation. DCA curves were plotted using the R package “ggDCA”.

Unsupervised clustering of samples and correlation analysis of the m6A hub gene

Because heterogeneity is prevalent among samples, unsupervised clustering of samples based on hub genes resolves this heterogeneity and is used to reclassify the samples. Concordant clustering of all samples was performed using the R package “Consensus-ClusterPlus” to select the optimal number of clusters based on scatter plots and concordance matrices, ultimately clustering samples into 2 classes. The expression profiles of the 10 hub genes in the two sets of samples are presented using a heatmap.

To resolve the correlation between these hub genes themselves, a correlation heatmap was drawn using the R package “corrplot”. In addition, to further investigate the correlation of these genes with ER stress and mitophagy processes, the related genes were retrieved from the GeneCards database with the keywords “endoplasmic reticulum stress” and “mitophagy”, respectively, and subsequently, the correlation between hub genes and these genes was calculated and visualized in the form of a

Ligamentum flavum hypertrophy on m6A and immune microenvironment

bubble plot. A scatter plot of correlations was drawn for the most significantly correlated hub gene pairs and fitted to the correlation curve.

Drug sensitivity analysis

Clinical drug resistance has always been one of the most important problems to solve in the field of clinical treatment. To reveal the relationship between these hub genes and the sensitivity to small molecule drugs, drug sensitivity data (IC50 values) from three databases, CCLE [29], CellMiner [30] and GDSC [31], were downloaded from the RNAactDrug database [32]. Subsequently, the correlation between the hub gene and small molecule drug IC50 values was calculated separately, and database by database display was performed using bubble plots.

Isolation, culture and identification of ligamentum cells

Ligament cells were isolated and cultured from patients with disc herniation and spinal stenosis according to previously described methods [33]. A total of 35 LFH and 28 nonligamentous hypertrophy patients were obtained from the seventh Affiliated Hospital of Sun Yat-sen University. The study was approved by the Ethics Committee of the seventh Affiliated Hospital of Sun Yat-sen University, and written consent was obtained from all patients. Briefly, fresh LF tissues were washed with PBS, cut and digested with collagenase type I after tissue shearing and mincing, and the digested tissue sections were then placed into Petri dishes as previously described [34]. The plates were incubated in an incubator (5% CO₂, 37°C). A small amount of DMEM containing serum was added and allowed to soak through the tissue pieces, but the tissue samples did not float. The flask was gently inverted, placed into an incubator at 37°C with 5% CO₂ and saturated humidity and allowed to stand. The medium was removed after 2 hours, and the flask was placed in position. An appropriate amount of DMEM containing penicillin, streptomycin and 10% fetal bovine serum was added to culture during passaging, and the fibroblast morphology of cultured cells was observed and identified by vimentin immunostaining and DAPI staining.

Cell monolayers were grown on cell climbing slides inserted into 12-well plates, and immunofluorescence staining was observed when

cells grew to approximately 70-80%. After washing with PBS, the cells were fixed in 4% paraformaldehyde in PBS for 20 min, washed with PBS, and mounted with PBS containing 0.5% Triton X-100 for 30 min at room temperature. Blocking was performed with 5% bovine serum albumin (BSA) in PBS for 1 h followed by staining with anti-vimentin monoclonal antibody (1 µg/ml; ab8978, Abcam Technologies) at 4°C overnight. A donkey anti-mouse IgG (H+L) highly cross-adsorbed secondary antibody was used after three washes (5 minutes each) in PBS (dilution 1:1000; A32744, Thermo Fisher Technologies). DAPI was used to stain the nuclei following sterile PBS washing, and the nuclei were mounted on coverslips with mounting solution overnight at room temperature. Images were acquired and analyzed using an LSM-880 laser confocal microscope system (Carl Zeiss CMP, Inc.).

Real-time quantitative polymerase chain reaction (RT-qPCR)

RT-qPCR was performed for all cell groups. According to the instructions of the Universal Column RNA Extraction Kit (R0027, Beyotime), total RNA was extracted and fractionated in 20 µl of total volume and subjected to reverse transcription to obtain cDNA, which was diluted to 100 µl. A total of 2 µl cDNA was used as a template for RT-qPCR (using an RT-qPCR kit, RR036B, Takara) amplification. The reaction conditions were as follows: 50°C for 2 min, 90°C for 2 min, 95°C for 15 s and 60°C for 1 min for 40 cycles. ACTA1 (5'-CATTACGAG-ACCACCTACAACAG-3' and 5'-GCCGATCCACACCGAGTATTTG-3'), MMP1 (5'-TTGGGCTGAAAGTGACTGGGAAAC-3' and 5'-GCTCTTGGCAAATCTGGCGTGTA-3'), MYL1 (5'-GTTGAGGGTCTGCGTGTCTTTGA-3' and 5'-GGGCTTCCACTTCTCTCTTTCAT-3'), MYOT (5'-TCGCAGCAACAACACTCAGAACAT-3' and 5'-GCAGTCCACTCACTTTGAGTCCAT-3'), POSTN (5'-TCATTGATGGAGTGCC-TGTGGAA-3' and 5'-GTGACCTTGGTGACCTCTTCTTGTA-3'), TNNC1 (5'-CTGTCTGACCTCTCCGCATGTT-3' and 5'-TCGTTGTTCTGTCTCCGTCCTC-3'), METTL16 (5'-TGTCACAGTACCATCACCAAGT-3' and 5'-ACGCCAGCACCACGATGTTATG-3'), PCIF1 (5'-TCAAGGTCAGCCGCAACTACT-3' and 5'-CACGCCGAACATCATCTGGTAC-3'), FTO (5'-CGGTATCTCGATCCTCATTGGTAA-3' and 5'-CACAGCATCCTCATTAGCCTTCTCT-3'), RUNX2 (5'-CACCCTCACTACCACACCTA-

Ligamentum flavum hypertrophy on m6A and immune microenvironment

CCT-3' and 5'-CTTCCATCAGCGTCAACACCATCA-3'), SP7 (5'-GCAAGAGGTTCACTCGTTCGGATG-3' and 5'-TCAGGTGGTTCGCTTCGGGTAAA-3'), OCN (5'-AGGGCAGCGAGGTAGTGA-3' and 5'-CC-TGAAAGCCGATGTGGT-3'), OPN (5'-CCGAGGTG-ATAGTGTGGTTTATGGA-3' and 5'-CCGAGGTG-ATAGTGTGGTTTATGGA-3') upstream and downstream primers were used at a final concentration of 500 nm each. GAPDH (5'-ACTTTG-TATCGTGAAGGACTCA-3' and 5'-CCAGTAGA-GGCAGGGATGATGTT-3') served as an internal reference for each group. The $2^{-\Delta\Delta CQ}$ method was used to calculate expression levels [35].

Total protein extraction and western blotting

After extraction with RIPA buffer (Thermo Fisher Scientific, USA), protein concentration was determined with a BCA Kit (Boster, China). A polyacrylamide gel containing SDS was electrophoresed and transferred to a polyvinylidene fluoride (PVDF) membrane. PVDF membranes were blocked with 5% skim milk (Solarbio, China) for 1 h before being incubated with primary antibodies overnight at 4°C, followed by secondary antibodies (conjugated with horseradish peroxidase) for 1 h at room temperature. A chemiluminescence kit (EpiZyme, China) was used to visualize the protein signals.

Statistical analysis

All data processing and analysis were performed using R software (version 4.0.2). For the comparison of continuous variables between two groups, the statistical significance of normally distributed variables was estimated by independent Student's t test, and differences between non-normally distributed variables were analyzed using the Mann-Whitney U test (i.e., Wilcoxon rank sum test). The chi square test or Fisher's exact test was used to compare and analyze the statistical significance between two groups of categorical variables. The Kruskal-Wallis test was used for comparisons of more than two groups, and the Wilcoxon test was used for comparisons between two groups. ROC curves were drawn using the pROC package of R, and the area under the curve (AUC) was calculated to evaluate the accuracy of the risk score to estimate prognosis. All statistical *P* values were two-sided, and $P < 0.05$ was considered statistically significant. Two-

tailed $P < 0.05$ was considered statistically significant.

Results

Data processing and differentially expressed gene analysis

Our workflow is shown in **Figure 1**. To study the effect of gene expression differences between LFH and normal tissues in the ligamentum flavum, we used the limma package on the GSE113212 gene expression matrix to analyze differential gene expression ([Supplementary Figure 1](#)). First, the gene expression matrix of the dataset was subjected to background correction and data normalization, and the gene expression before and after data normalization is displayed in a box diagram ([Supplementary Figure 1A](#) and [1B](#)). *P* value < 0.05 and $|\log_2FC| > 1$ (i.e., 2-fold significant difference) served as the threshold, and 1259 differential genes were identified in the comparison between hypertrophic ligamentum flavum and normal tissues, including 471 upregulated genes and 788 downregulated genes. Divergently expressed genes (DEGs) upregulated and downregulated shown by the volcano map can be easily distinguished ([Supplementary Figure 1C](#)). The heatmap ([Supplementary Figure 1D](#)) was drawn by using differentially expressed genes and data grouping. Differentially expressed genes effectively distinguish hypertrophic tissue and normal tissue of the ligamentum flavum.

The landscape of m6A regulators between normal and LFH samples

Next, all m6A genes were visualized for expression dissimilarity in normal and disease samples by plotting heatmaps and grouped box plots (**Figure 2A, 2B**). Of the three m6A genes, reader was less discriminative than writer and eraser, and a total of three genes showed significant differences ($P < 0.05$) between the two samples (METTL16, PCIF1, and FTO). In addition, we also assessed the localization of these genes in chromosomes and plotted a panoramic view of the localization of genes on chromosomes in combination with multiple ring presentations (**Figure 2C**). The results showed that some genes were near the chromosome; thus, these genes were closely linked at the genomic level.

Ligamentum flavum hypertrophy on m6A and immune microenvironment

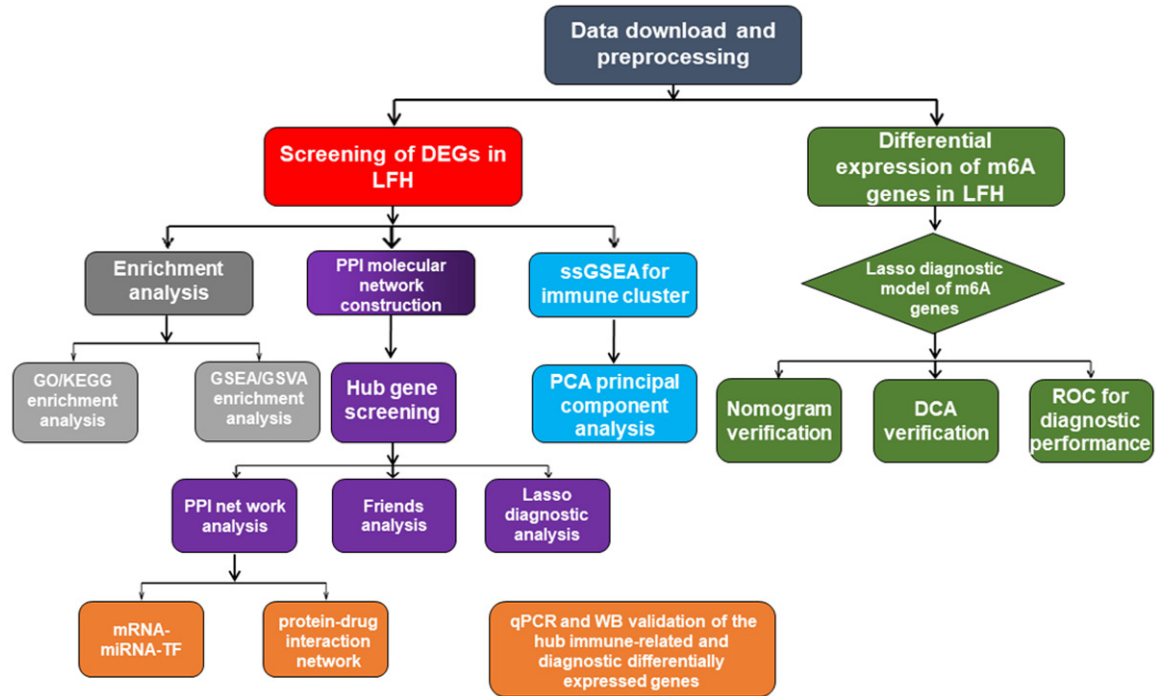


Figure 1. The flow-process diagram for screening datasets. m6A: N6-methyladenosine; LFH: Ligamentum Flavum Hyperplasia; GO: Gene Ontology; KEGG: Kyoto Encyclopedia of Genes and Genomes; GSEA: Gene Set Enrichment Analysis; PPI: Protein-Protein Interactions; Lasso: Least absolute shrinkage and selection operator; GSVA: Gene Set Variation Analysis; PCA: Principal Component Analysis; ROC: Receiver Operating Characteristic; DEGs: Differentially Expressed Genes; ssGSEA: single-sample Gene Set Enrichment Analysis; RT-qPCR: Real-Time quantitative PCR; WB: Western Blotting.

GO term and KEGG pathway enrichment analysis

We compared the DEGs between the hypertrophic ligamentum flavum sample and the normal sample group. The cluster profiler package was used for GO and KEGG pathway enrichment analyses. $P < 0.05$ (adjusted) and a Q value < 0.05 were considered to indicate significantly differentially expressed genes. The enrichment results are shown in bar charts (Figure 3A, 3B). Supplementary Table 1 shows the GO enrichment entries of significance for the top 20. GO enrichment analysis showed that the differentially expressed genes were enriched in bone development, bone reconstruction and regulation, bone and biomineral tissue development, ossification, cartilage development and cell differentiation, muscle system and muscle contraction, myosin complex and myofibril, immune receptor activity, oxidoreductase activity, leukocyte migration and transforming growth factor β . Supplementary Table 2 shows the results of KEGG enrichment

analysis, showing that differential genes are enriched in protein digestion and absorption, tyrosine metabolism, cytokine-cytokine receptor interaction, rheumatoid arthritis, osteoclast differentiation, proteoglycans in cancer, complement and coagulation cascade, PI3K-Akt, PPAR signaling pathway and other pathways (Supplementary Figure 5A-E).

GSEA and GSVA suggest that immune-related factors play an important role

To determine the effect of gene expression level on ligamentum flavum hypertrophy, we analyzed the gene function, biological pathway, and molecular characteristics of gene expression in the two groups of data. We used a heatmap to show the results. Regarding gene function in GSE113212 data, the differentially expressed genes are mainly involved in enzyme activator activity, cell migration, regulation of immune cell activation, angiogenesis, skeletal system development, etc. The main pathways affected were the PPAR signaling pathway,

Ligamentum flavum hypertrophy on m6A and immune microenvironment

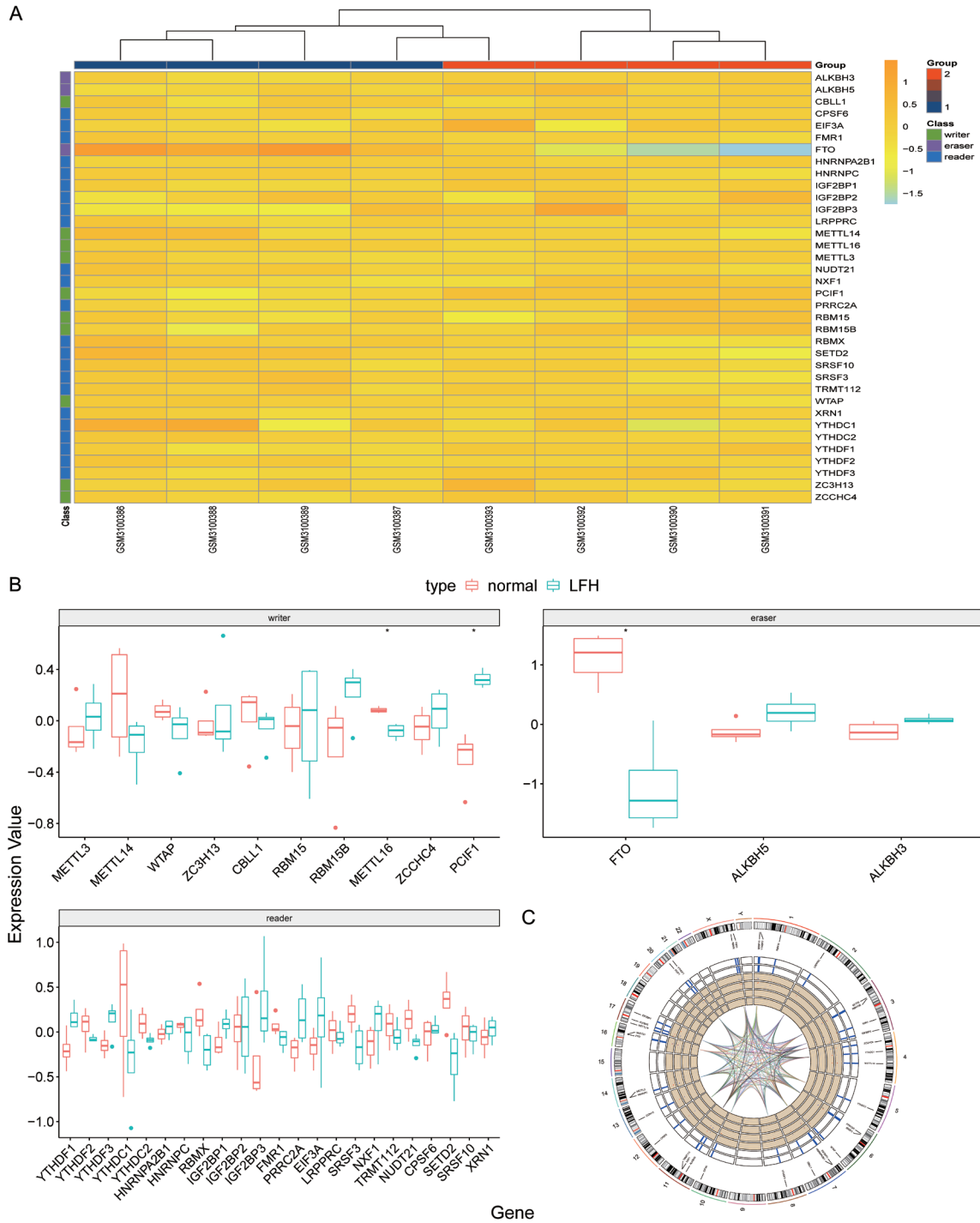


Figure 2. m6A gene panorama. A. m6A gene differential expression heatmaps, behaving genes, listed as samples, as well as different types of genes are labeled using different color blocks. Red represents high expression values and blue represents low expression values in the graph; B. m6A genes are differentially expressed box plots, with the x-axis as genes and the y-axis as gene expression values, with sample groupings distinguished by different colors and binned by gene type, box plots with the middle line as the median value, the upper box line as the upper quartile, and the lower box line as the lower quartile, and statistical tests were performed by Wilcoxon rank sum test, and the upper symbols represent the level of significance of the difference, * $P < 0.05$, ** $P < 0.01$; *** $P < 0.001$; **** $P < 0.0001$; C. A ring diagram of chromosomal localization. Circles 2 and 3 represent gene corresponding expression heatmaps, red represents high expression, blue represents low expression, circles 4 and 5 represent gene corresponding expression scatter plots, circles 6 and 7 represent expression histograms, and the innermost network consists of two connections of reader genes, representing close links of these genes. m6A: N6-methyladenosine.

Ligamentum flavum hypertrophy on m6A and immune microenvironment

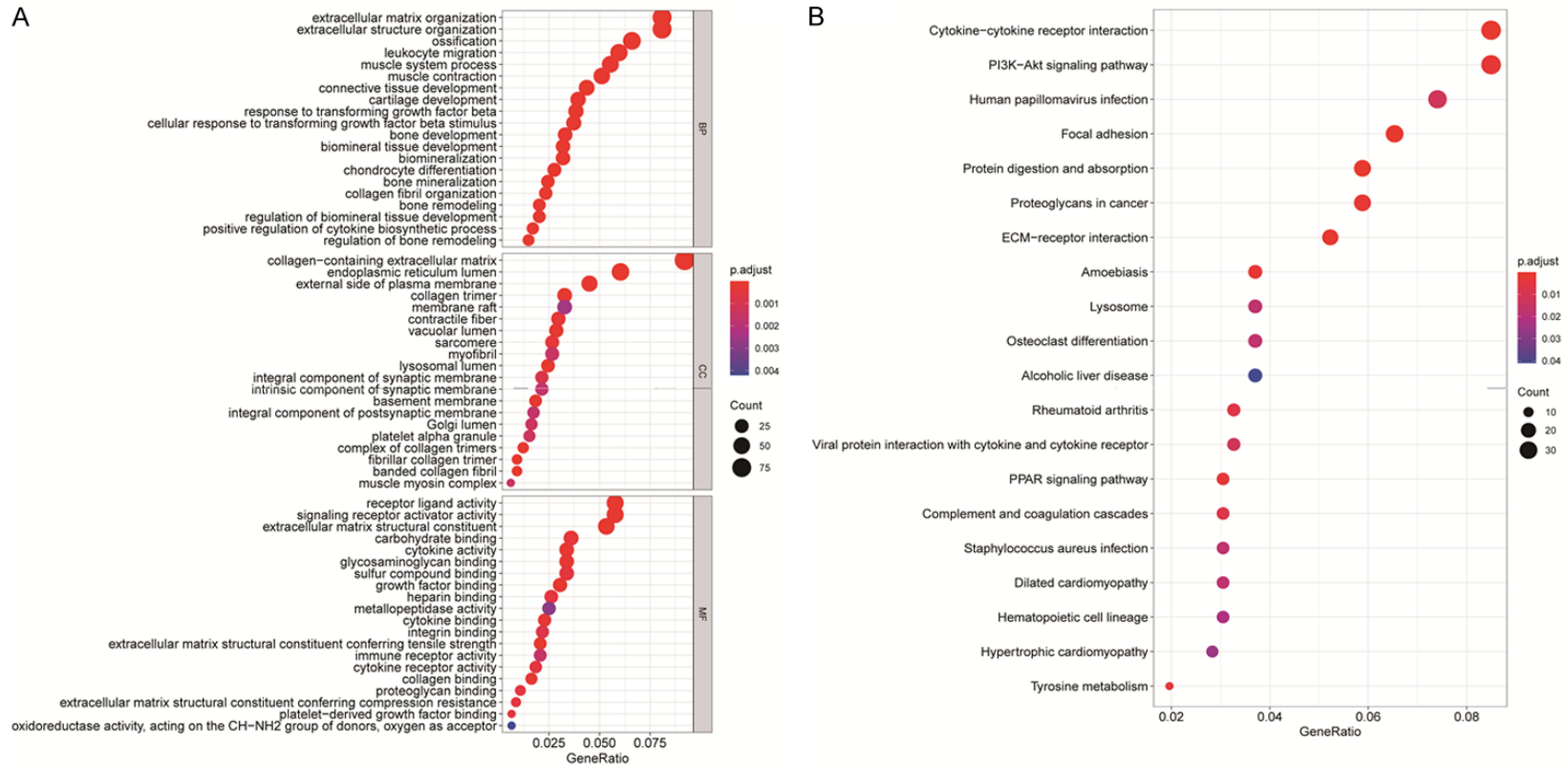


Figure 3. GO analysis of DEGs between the hypertrophy and normal sample groups of ligamentum flavum is shown in (A, B) GO entry enrichment bubble plot between FBXL7 high expression group and low expression group in TCGA-BLCA dataset. GO: Gene Ontology; DEGs: differentially expressed genes.

Ligamentum flavum hypertrophy on m6A and immune microenvironment

AMPK signaling pathway, cGMP PKG signaling pathway, Th17 cell differentiation, Relaxin signaling pathway, cell adhesion molecules and axon guidance-related pathways (**Figure 4A-D**). The molecular characteristics of GSEA enrichment were characterized by the enrichment of immunomodulatory interactions between lymph and nonlymphocytes, protein metabolic regulation, and antigen processing and presentation (**Supplementary Figure 6A-C**), which is consistent with the previous enrichment results. See **Supplementary Tables 3, 4** for the detailed results.

We also performed GSVA enrichment analysis between groups. The background set was displayed in the form of a bar graph and heatmap (**Figure 5A, 5B**) and a grouping box graph (**Figure 5C**) using the `msigdb.v7.0.symbols.gmt` pathway set and immune-related characteristic gene set, respectively. The results showed that hypertrophy in the senile ligamentum flavum mainly affected biological-related pathways, such as DNA repair, myogenesis, glycolysis, inflammatory response, and hormone response. As a result, ligamentum flavum hypertrophy enriches some immune-related signaling pathways, implying an important role for immune factors.

ssGSEA and evaluation of immune cell infiltration

Enrichment analysis results revealed significant differences in the immune process between the two groups of samples. Therefore, to further analyze the immune infiltration level between the two groups of samples, we performed ssGSEA on the GSE113212 dataset to evaluate the degree of immune cell infiltration. The scores of 28 immune cells of all samples were calculated and clustered using the ssGSEA method, and the samples were hierarchically clustered by the `hclust` function. The sample was divided into three groups of high, medium, and low immune scores and displayed in a tree view (**Figure 6A**). The ssGSEA immune infiltration score of each sample in 28 immune cells (**Figure 6B**) and the expression of 28 immune cells in the high, medium and low immune score groups (**Figure 6C**) are displayed in a heatmap. The box chart shows the difference in the immune score of the high, medi-

um and low immune score groups in the immune.gmt immune-related gene set (**Figure 6D**).

To assess the reproducibility of the data within the normal group and LFH group, we performed principal component analysis (PCA), and we plotted a PCA cluster based on the between-group differences in LFH and the degree of differential immune cell infiltration assessed by ssGSEA. The results showed that the data were reproducible in GSE113212 (**Figure 7A**). The analysis between the hypertrophic ligamentum flavum and the normal ligamentum (**Figure 7B**) and the high and low immunoscore groupings (**Figure 7C**) were analyzed according to the immune infiltration score results obtained from ssGSEA.

Construction of molecular interaction networks and immune-related diagnostic models for LFH

According to the immune infiltration score cluster grouping derived from the above ssGSEA, three group clusters with high and low immune scores were analyzed using the `limma` package for pairwise comparison of DEGs between groups, and a total of 473 DEGs were obtained. Using the STRING database and Cytoscape, we constructed a PPI network (**Figure 8A**). Subsequently, we visualized the HubGenes of the CytoHubba plug-in MCC algorithm top 30 (**Figure 8B**) together with the most connected set of HubGenes obtained from MCODE plug-in analysis (**Figure 8C**). To identify the intersection of significant nodes of CytoHubba and MCODE screening to obtain 16 HubGenes, an LFH immune-related diagnostic model was constructed based on the HubGenes (**Supplementary Figure 2A**). Regression screening was first performed using the Lasso method, and the optimal lambda value was determined with a total of 6 genes remaining after screening (**Supplementary Figure 2B, 2C**). We plotted the differential expression of six LFH immune-related prediction model genes ACTA1, MMP1, MYL1, MYOT, POSTN, and TNNC1 in LFH (**Figure 9**).

We constructed mRNA-miRNA-TF molecular networks for 16 HubGenes (**Figure 10A**). The DrugBank database was also used to construct a protein drug interaction network (**Figure 10B**). Among the 16 HubGenes, only the proteins expressed by the differentially expressed

Ligamentum flavum hypertrophy on m6A and immune microenvironment

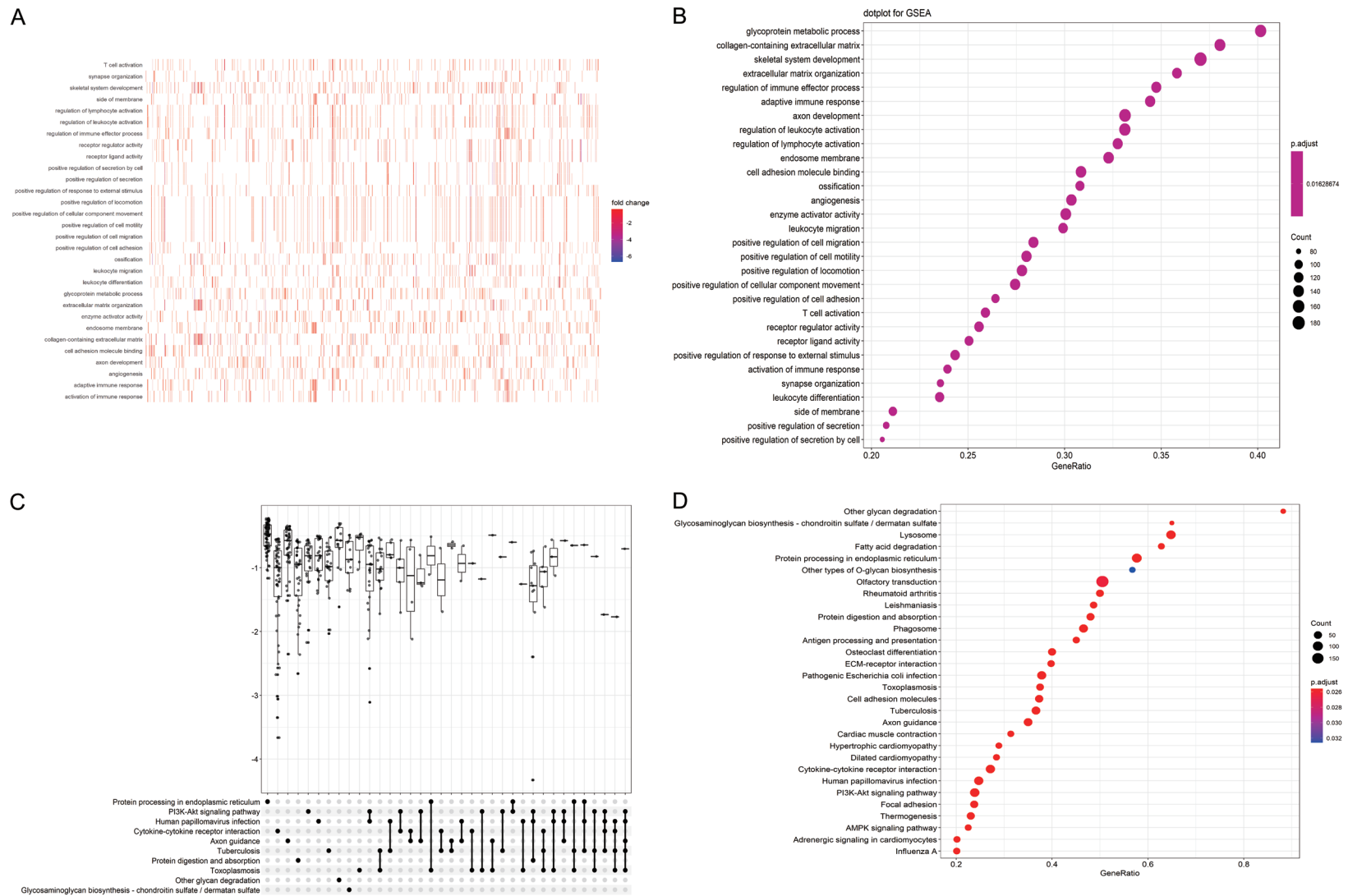


Figure 4. GSEA enrichment analysis. A, B. Molecular functional heat map and bubble map of GSEA enrichment analysis; C, D. Upset diagram and Bubble Diagram of GSEA enrichment analysis impact pathway. GSEA: Gene Set Enrichment Analysis.

Ligamentum flavum hypertrophy on m6A and immune microenvironment

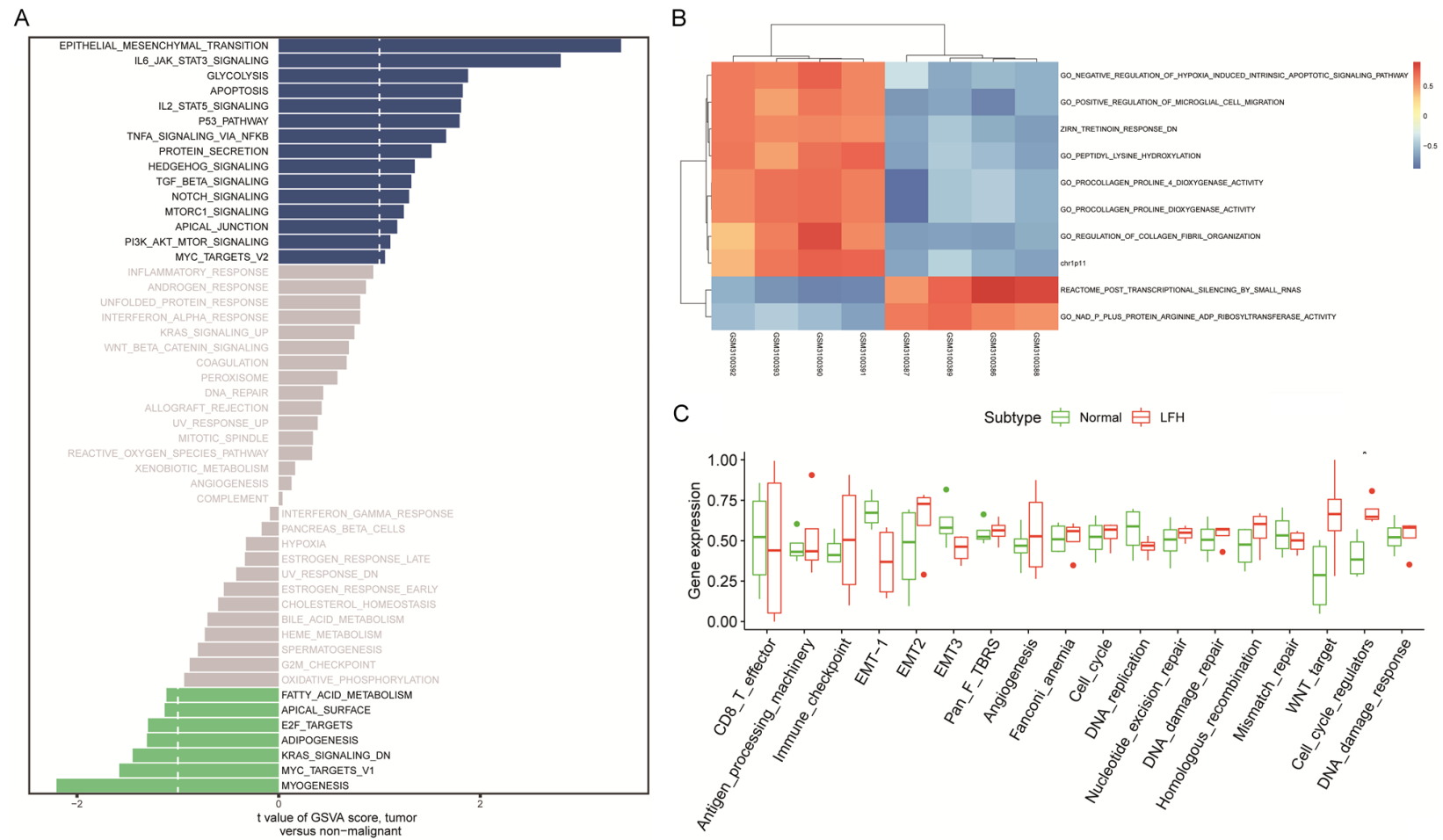


Figure 5. Enrichment analysis of GSVA. A, B. GSVA enrichment analysis of msigdb.v7.0.symbols.gmt pathway set, showing the enrichment results of genes in GSE113212 data in the form of bar graph and heat map; C. Enrichment results of immune related characteristic genes in GSE113212 data. GSVA: Gene Set Variation Analysis.

Ligamentum flavum hypertrophy on m6A and immune microenvironment

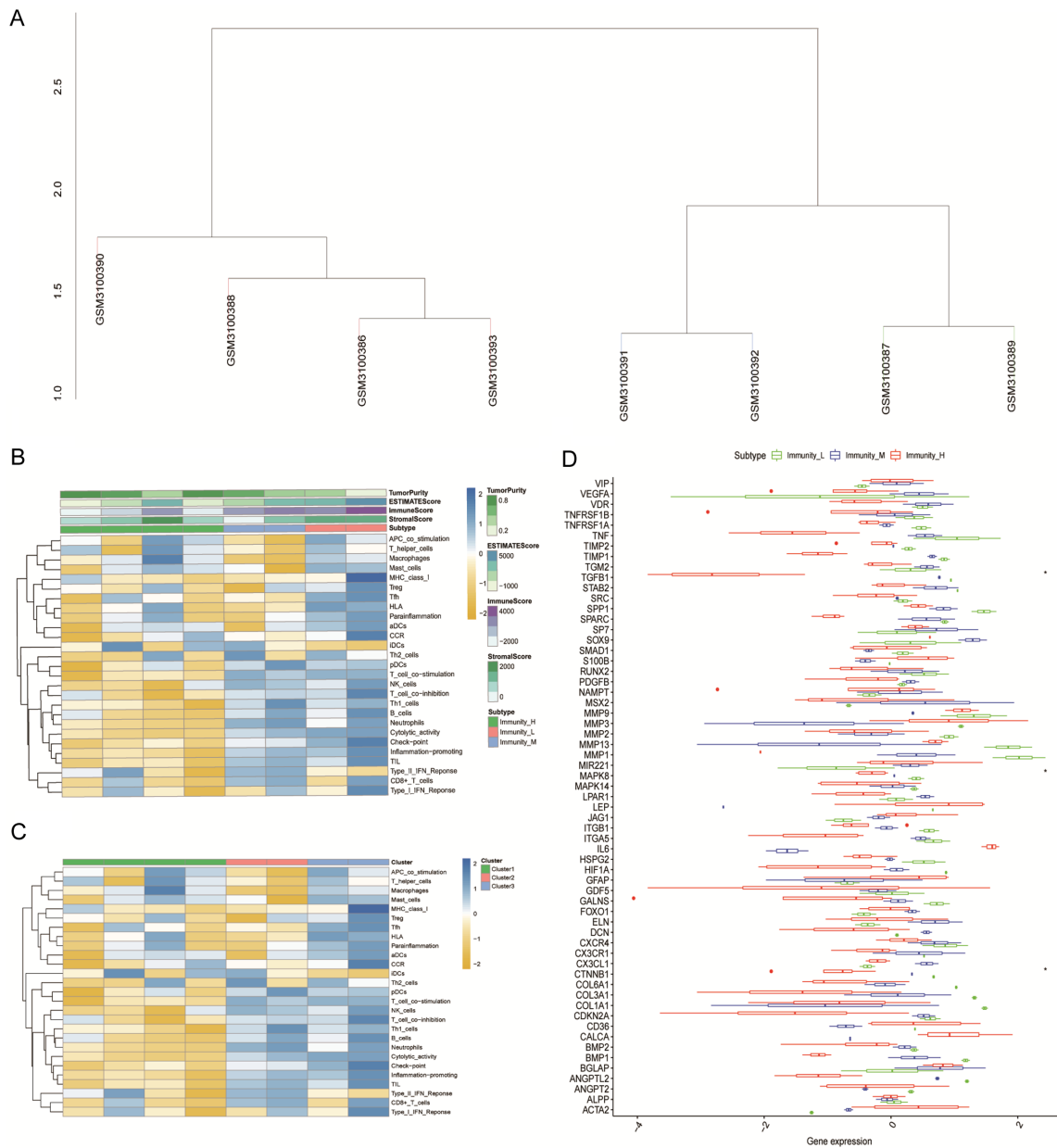


Figure 6. ssGSEA immune infiltration assessment. **A.** Immune clustering grouping of 8 samples in the data set; **B.** Heatmap of ssGSEA immune infiltration score in 28 immune cells of each sample; **C.** The expression heat map of 28 immune cells in high, medium and low immune score groups; **D.** Immune score box diagram of immune related gene set. The x-axis is the immune cells at the level of immune infiltration, and the y-axis is the immune gene in immune.gmt. Each color represents the grouping of high, medium and low immune scores. The statistical test method is Wilcoxon rank sum test. The symbol above represents the significance level of difference, * $P < 0.05$, ** $P < 0.01$; *** $P < 0.001$, **** $P < 0.0001$. ssGSEA: single-sample Gene Set Enrichment Analysis.

genes are shown centrally, and these genes are drug targets. These drugs may have some effects on the occurrence and development of LFH. These 3 genes have the potential to differentiate between the hypertrophic group of the ligamentum flavum and normal ligamentum

teres. We also performed Friends analysis on 16 Hub differential genes immunologically related to ligament hypertrophy. TCAP showed the strongest correlation with other genes and might be involved in a variety of functions (**Figure 10C**).

Ligamentum flavum hypertrophy on m6A and immune microenvironment

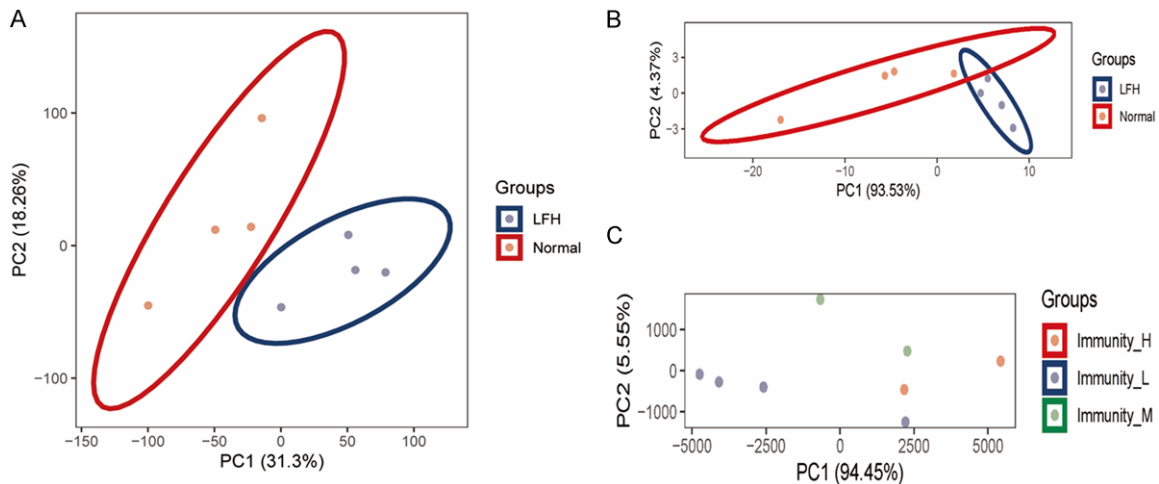


Figure 7. PCA principal component analysis. A. Principal component analysis between the normal ligament groups of the normal and LFH patients in the GSE113212 dataset, which was reproducible; B. Principal component analysis of immune infiltration scores derived from ssGSEA analysis between the aged and young normal ligament groups with ligamentum flavum hypertrophy was reproducible and good; C. High and low immunoscore group principal component analysis with good reproducibility. LFH: Ligamentum Flavum Hyperplasia; PCA: Principal Component Analysis; ROC: Receiver Operating Characteristic; DEGs: Differentially Expressed Genes; ssGSEA: single-sample Gene Set Enrichment Analysis.

Four m6A gene-based diagnostic models

Given that m6A-regulated gene expression is of great biological significance, we further analyzed whether the occurrence of LFH is affected by m6A gene-related mechanisms. We further constructed a predictive diagnostic model of LFH disease for the 37 m6A genes. Similarly, m6A genes were first filtered using the method of Lasso regression to remove genes with no coefficient contribution to the diagnostic model and determine the optimal lambda value with a total of 4 genes remaining after screening (Figure 11A, 11B). Subsequently, a forest plot was used to visualize 4 diagnostic models composed of m6A genes (Figure 11C). The results showed that the genes with the largest absolute impact coefficients in this model were mettl16 with an impact coefficient of 18.22.

Subsequently, to verify the accuracy of the model, we first selected the above 4 genes with the factors of age and sex to construct a multivariate logistic model, which was visualized using a nomogram (Supplementary Figure 3A). The results showed that 4 genes affected the prediction model to a much greater extent than age and sex, which highlighted the precision of the model. Then, the predictive efficacy of the model was further validated using recall

curves, ROC curves of single genes and DAC curves (Supplementary Figure 3B-D). The results showed that the model achieved superior predictive efficacy and robustness in all three validation modalities (Supplementary Figure 3E-H). Presents single-gene ROC curves for the 4 genes to exemplify the superior diagnostic efficacy.

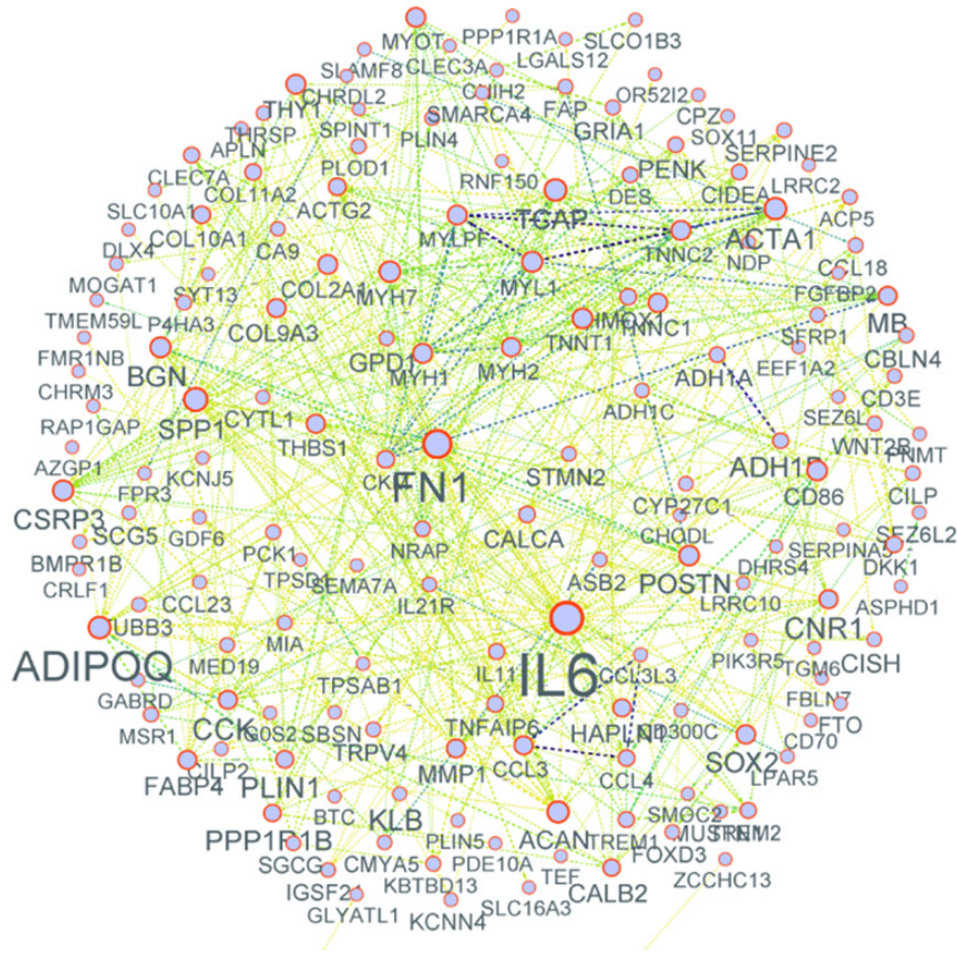
To further analyze the m6A writer and eraser gene expression links, we calculated pairwise correlations and plotted a scatter plot of correlations and fitted correlation curves. We identified a total of three gene pairs with a correlation of $R > 0.7$ that met the statistical significance threshold: METTL3-ZC3H13, ZC3H13-CBLL1, and METTL3-CBLL1 (Supplementary Figure 4). Of these, 2 pairs were negatively correlated, and 1 pair was positively correlated.

Correlation analysis of hub m6A genes of LFH

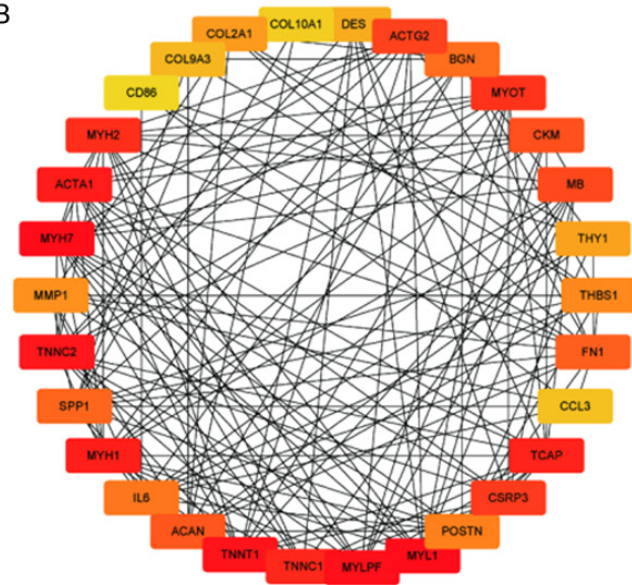
Hub m6A genes tend to be from the same family and were more closely and significantly related. We therefore calculated the top 10 most connected genes among 37 m6A genes by CytoHubba as hub m6A genes (Figure 12A, 12B) and analyzed their pairwise correlation (Figure 12D). Due to the prevalent heterogeneity among samples, we performed unsupervised clustering of samples according to the

Ligamentum flavum hypertrophy on m6A and immune microenvironment

A



B



C

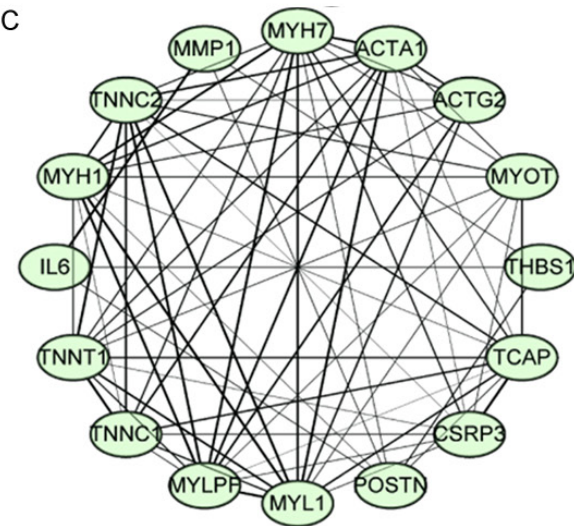


Figure 8. Construction of DEGs molecular interaction network and HubGene screening between ligamentum flavum hypertrophy and normal sample groups. A. Protein protein interaction network of the ligamentum flavum hypertrophy related differentially expressed genes; B. The top 30 significant nodes in the protein interaction network were screened by CytoHubba software; C. Identification of key modules in the protein interaction network 1 by MCODE. DEGs: Differentially Expressed Genes; MCODE: Molecular Complex Detection.

Ligamentum flavum hypertrophy on m6A and immune microenvironment

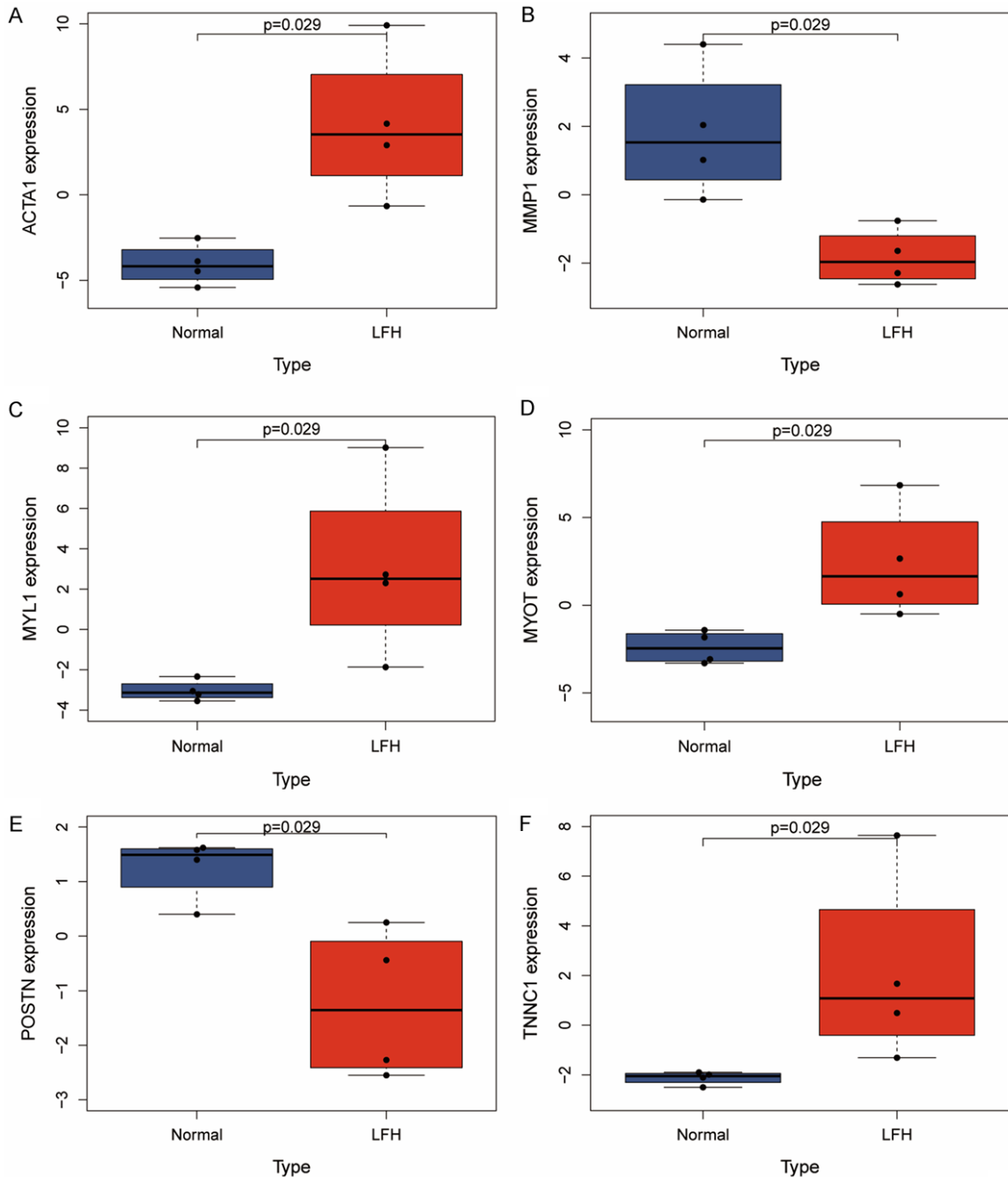


Figure 9. Prediction model for differential gene expression. Differential expression of 6 LFH immune-related prediction model genes ACTA1 (A), MMP1 (B), MYL1 (C), MYOT (D), POSTN (E), TNNC1 (F) in LFH. LFH: Ligamentum Flavum Hyperplasia.

expression of m6A genes, clustering the samples into 2 categories. The expression profiles of the 10 hub genes in the two sets of samples were displayed using a heatmap (**Figure 12C**). YTHDC1 showed significant positive correlations with METTL14 and YTHDC2, with correlation coefficients of 0.810 and 0.714, respectively (**Figure 12E, 12F**).

Hub m6A gene and drug sensitivity analysis of LFH

To reveal the relationship between these 10 hub m6A genes and small molecule drug sensitivity, data from three drug sensitivity databases were integrated, and a bubble plot of the correlation relationship between gene expres-

Ligamentum flavum hypertrophy on m6A and immune microenvironment

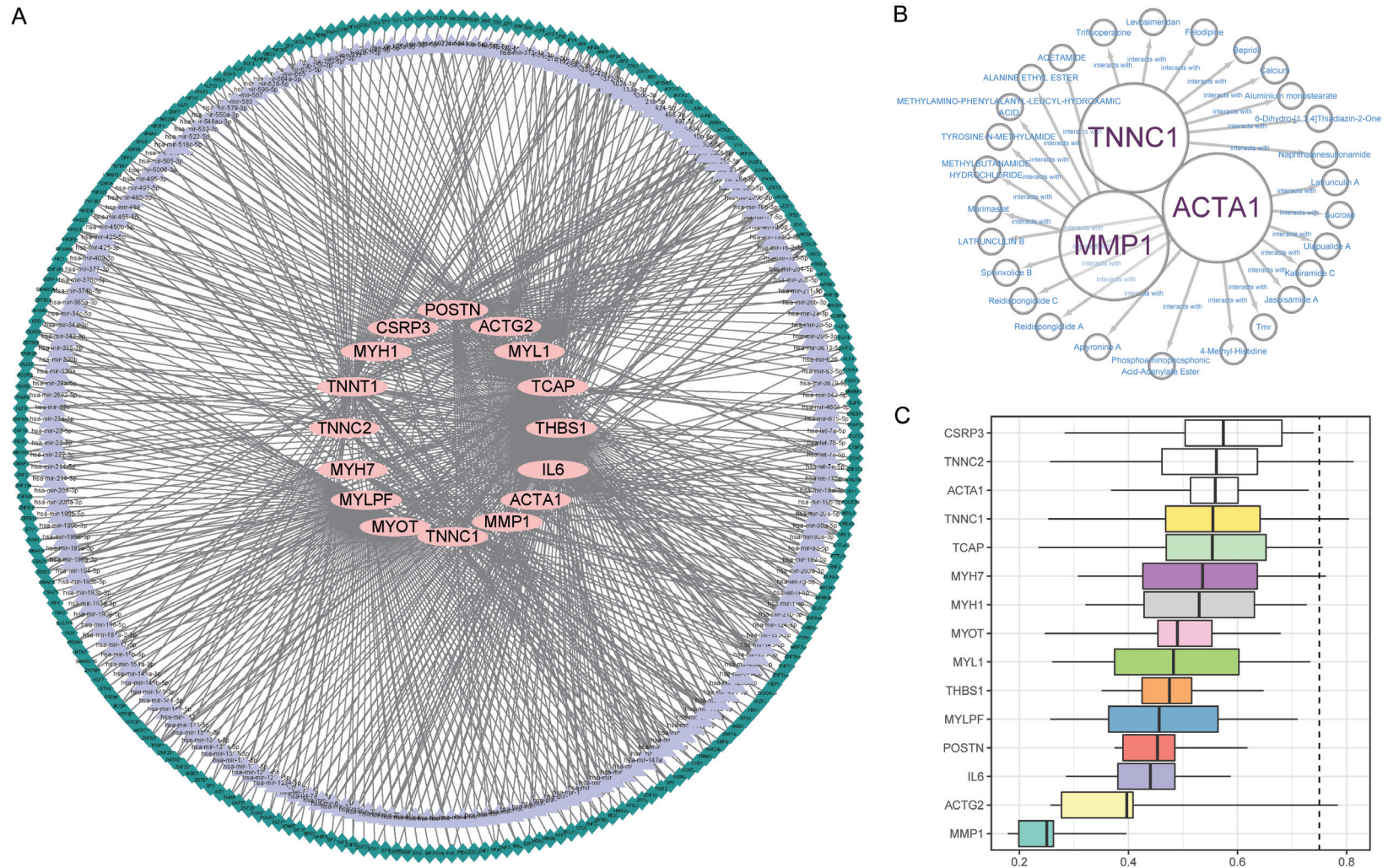
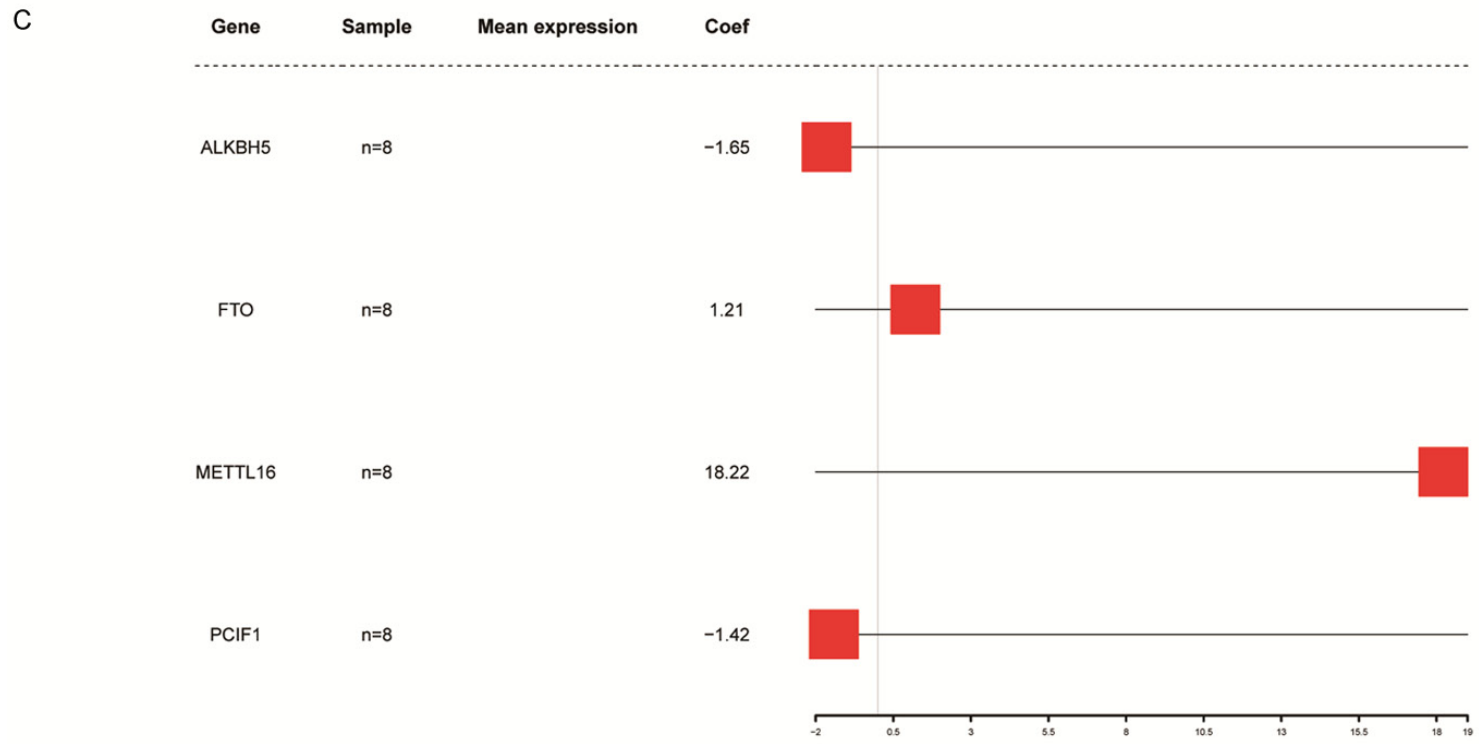
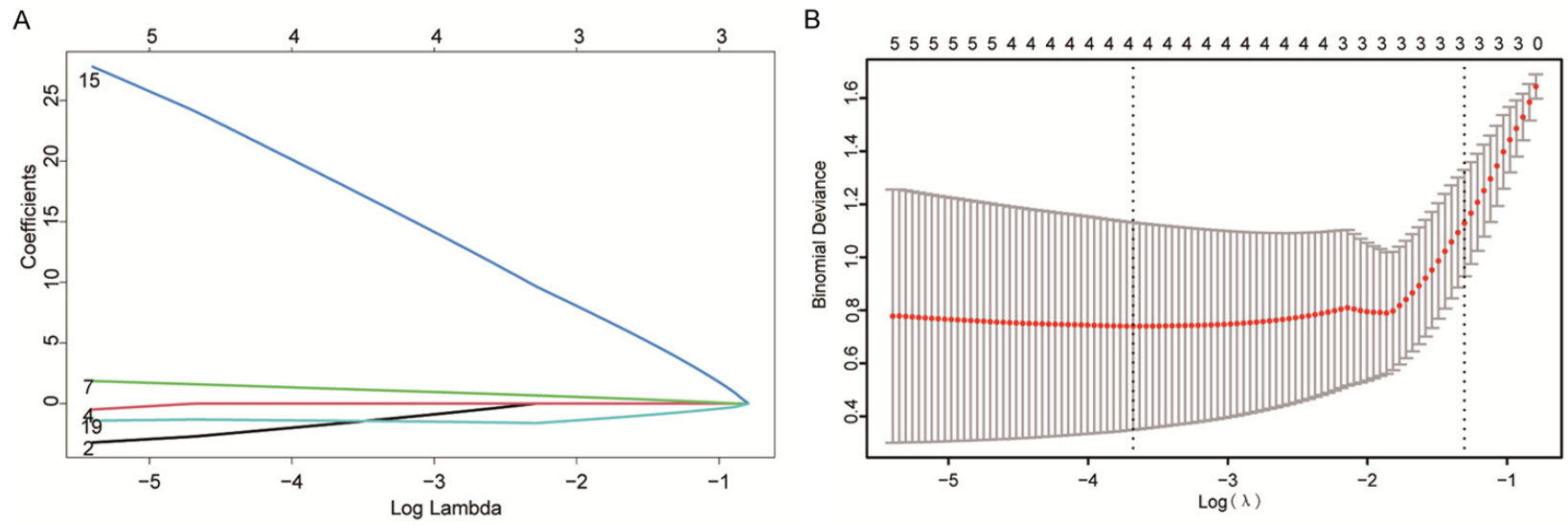


Figure 10. PPI network construction of 16 hub genes. A. MRNA-miRNA-TF molecular network with Hub Genes in pink, TF in purple, and miRNA in green; B. The protein drug phase interaction network was constructed through the DrugBank database; C. Ligamentum hypertrophy immune related 16 Hub differential genes friends analysis, box plots demonstrating the functional similarity scores between the differentially expressed genes immune related to ligamentum flavum hypertrophy. PPI: Protein-Protein Interactions.

Ligamentum flavum hypertrophy on m6A and immune microenvironment



Ligamentum flavum hypertrophy on m6A and immune microenvironment

Figure 11. A. Lasso regression curves. This figure demonstrates the convergent screening process of lasso regression on 29 gene features, with the x-axis as the log lambda value, the y-axis as the regression coefficient, and differently colored lines representing different features. B. Lambda value selection curves. This plot was used to select the optimal lambda value for the lasso regression model, typically taking the lowest point, which is the optimal lambda value at the dotted left side of the plot. C. Forest plot of diagnostic model. The first column is represented by the 4 genes comprising the model, the second by the number of samples, the third by the mean expression value of these genes, and the fourth column and corresponding graph are the coefficients of influence of these genes in the model.

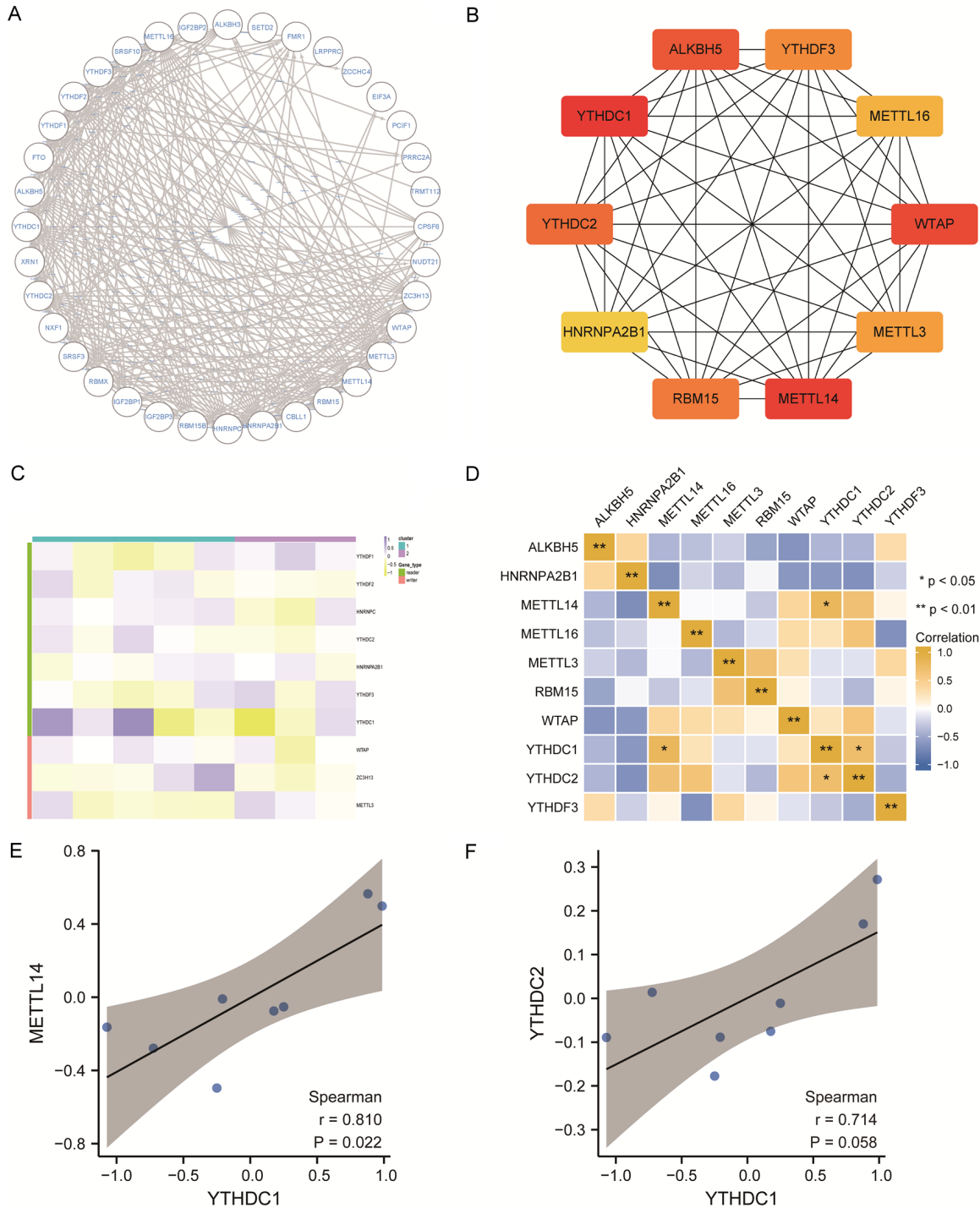


Figure 12. Correlation analysis of hub m6A gene. A. Protein protein interaction network of m6A genes; B. Top 10 significant nodes in protein interaction networks were screened by CytoHubba software; C. m6A gene associated

Ligamentum flavum hypertrophy on m6A and immune microenvironment

samples unsupervised clustering Heatmap of differences in hub m6A genes between groups; D. Heatmap of correlations among hub m6A genes; E, F. Scatter plots of correlation of gene YTHDC1 with gene METTL14, gene YTHDC2. Each point in the figure represents one sample, the straight line is the correlation fitting curve, and the shaded portion is the confidence interval. m6A: N6-methyladenosine.

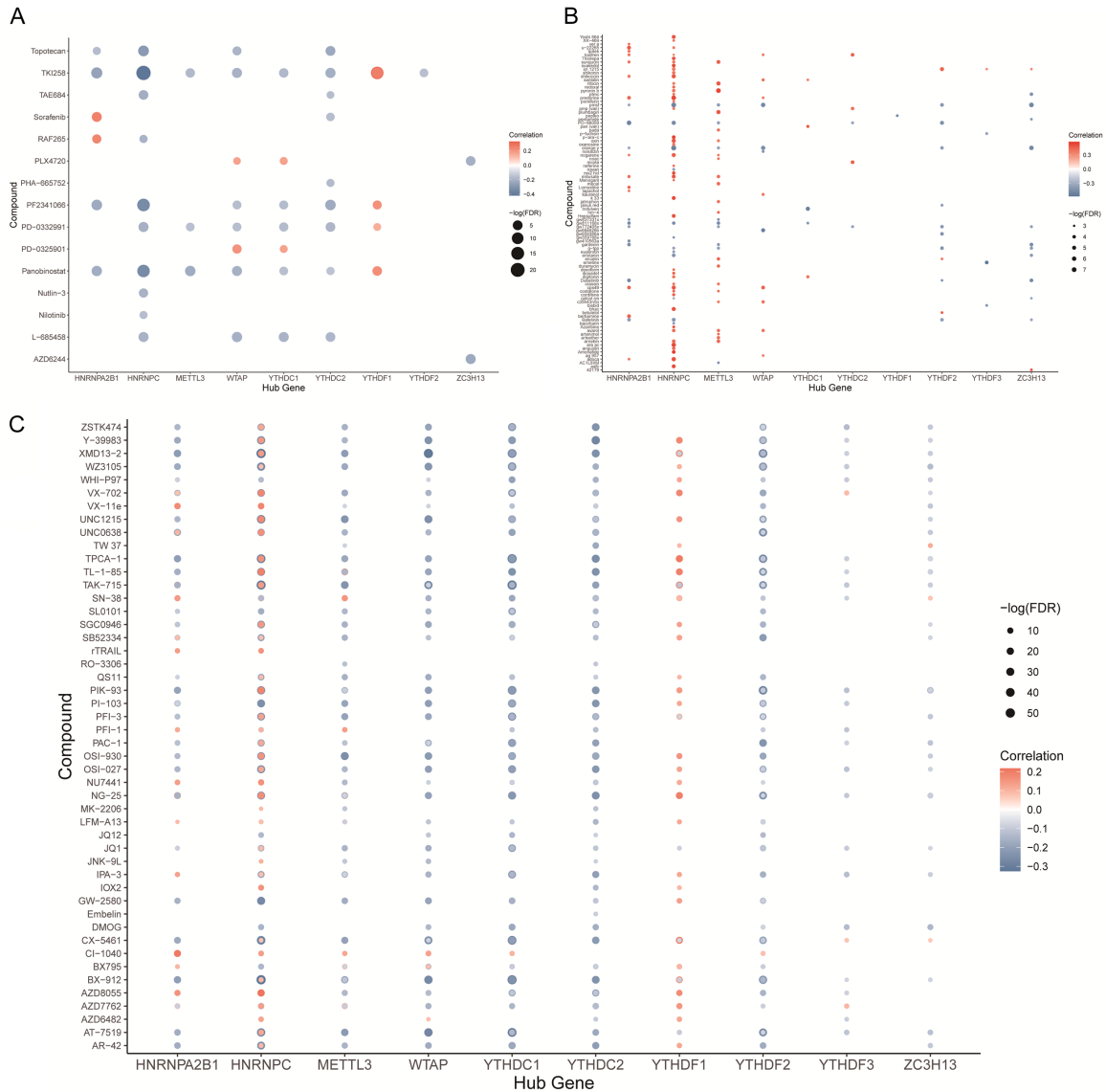


Figure 13. Drug sensitivity analysis. A. Drug sensitivity analysis bubble plot of the CCLL database. B. Drug sensitivity analysis bubble plot of the CellMiner database. C. Drug sensitivity analysis bubble plot of the GDSC database.

sion values and IC50 values of small molecule drugs was separately drawn (Figure 13). A higher IC50 value represents a higher level of drug resistance. Thus, a positive correlation indicates that elevated expression of this gene will be able to enhance drug resistance, whereas a negative correlation represents a lower level of drug resistance as the gene expression value increases. According to the CellMiner database, the HNRNPC gene is positively correlated with the vast majority of small molecule drugs, 8819

indicating that its high expression increases the drug resistance of a significant number of these drugs.

Validation of the differential expression of m6A-related genes in LFH patients - a prospective analysis in a new population

To validate the reliability of the GSE113212 dataset, we acquired fibroblasts from the ligamentum flavum in clinical samples (Figure 14A), which were used at the P3 generation for Am J Transl Res 2022;14(12):8800-8827

Ligamentum flavum hypertrophy on m6A and immune microenvironment

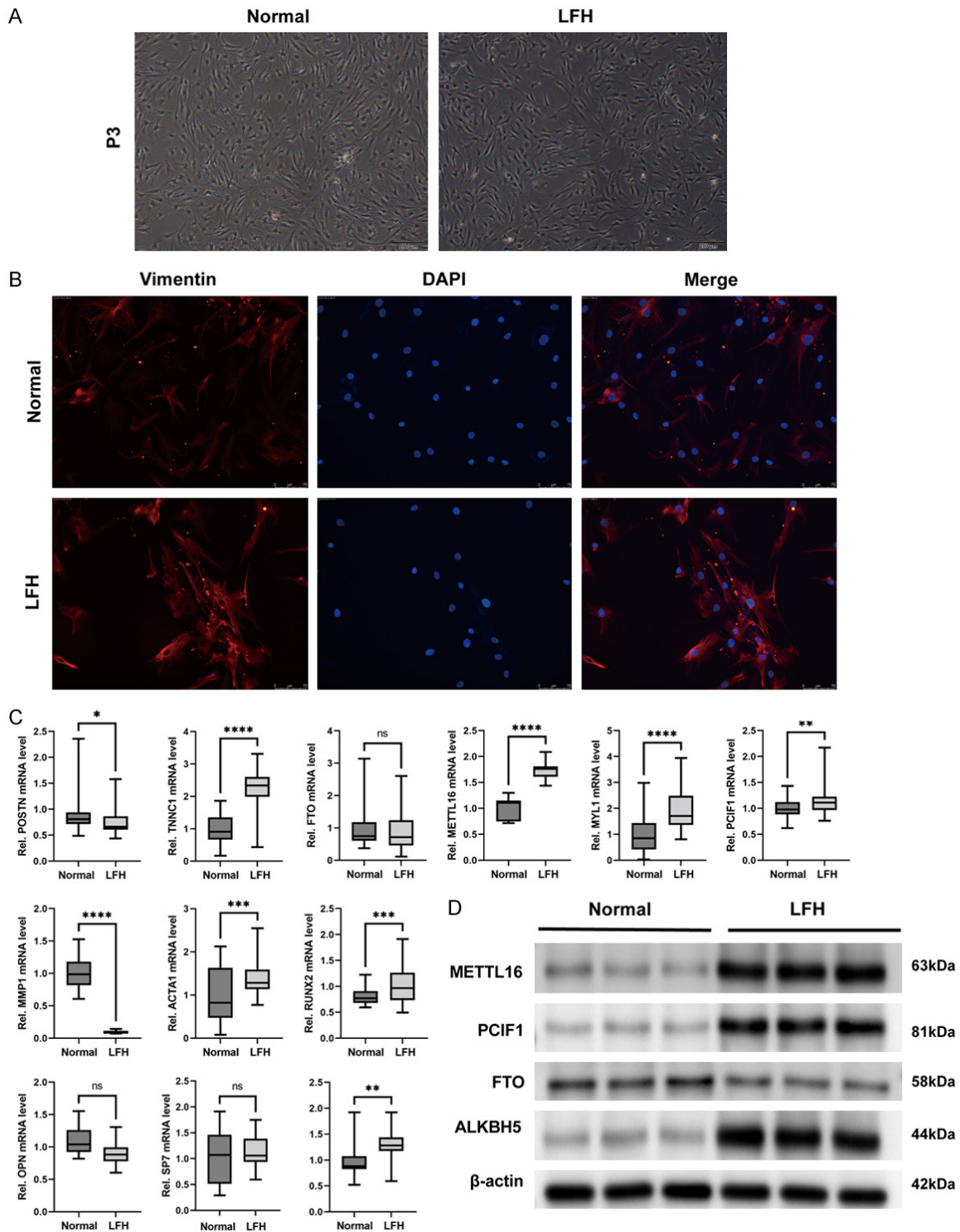


Figure 14. The RNA expression of related genes was identified and measured in LFH and non-LFH samples. A, B. Ligament cells were obtained by enzymatic digestion using LFH and non-LFH samples, P3 generation cells were used for experiments, and vimentin antibody pairs were used to identify fibroblasts. C. RT-qPCR was used to detect the RNA expression of POSTN, TNNC1, FTO, METTL16, MYL1, MMP1, PCIF1, ACTA1, RUNX2, SP7, OCN and OPN in cell samples. *P*-values were calculated using a two-sided unpaired Student's *t*-test. ***P* < 0.01; ****P* < 0.001; *****P* < 0.0001. D. Reduced FTO expression and up-regulated METTL16, PCIF1, and ALKBH5 levels in LFH were validated by Western blotting. LFH: Ligamentum Flavum Hyperplasia.

the trial and confirmed by vimentin immunofluorescence staining (**Figure 14B**). The expression levels of nine differentially expressed m6A-related genes were further determined by RT-qPCR. Similar to the results of mRNA microarrays in LFH samples, expression levels of TNNC1, METTL16, MYL1, PCIF1, ACTA1, RUNX2 and OCN were significantly higher in LFH samples than in normal samples. Furthermore, there was a significant decrease in the expression levels of POSTN and MMP1. FTO, MYOT, SP7, and OPN expression levels were not significantly different between the two groups (**Figure 14C**). Four diagnostic model genes of m6A were further determined by western blotting, among which the expression of METTL16, PCIF1, ALKBH5 was increased and the expression of FTO was decreased in LFH (**Figure 14D**).

Discussion

LFH is a chronic progressive disease, and surgical treatment for patients with severe symptoms is the mainstream treatment. Inflammation appears to be one of the most important events in fibrosis, and chronic inflammation plays a role in progressive LF fibrosis as well. Current evidence confirms the indispensable role of m6A modification in innate and adaptive immune responses, suggesting that the immune microenvironment of LFH needs to be further explored [36, 37]. Several studies have addressed the role of m6A in immunity, particularly in infiltrating cells of the tumor microenvironment [38]. The potential regulatory mechanisms of m6A-related regulators in LFH timing and immune response need to be further investigated. Therefore, the search for novel serologic or histologic prognostic markers has potential value for diagnosis, prognosis, and treatment. A comparison of LFH and normal ligament tissues revealed differences in m6A-related gene expression. Also, the immune microenvironment and m6A-related gene expression levels were examined in LFH. This finding implied that the disruption of the RNA methylation system may play a critical role in the progression of LFH.

Increasing evidence suggests that m6A modification plays an indispensable role in innate and adaptive immune responses. Our GO analysis results showed that immune-related pathways were mainly enriched in LFH samples and were

related to osteogenesis and chondrogenesis, migration of immune cells and activity of immune receptors. Through mRNA verification, we showed that the osteogenic indexes (RUNX2 and OCN) of fibroblasts in LFH patients were higher than those in normal ligamentum flavum group, suggesting that ligament cells in LFH patients have the potential of further osteogenesis. KEGG enrichment analysis indicated that the PI3K-Akt and PPAR signaling pathways were primarily enriched in immune-related pathways. In addition, we conducted GSEA and GSVA and found that the identified genes are characterized by enrichment of immunoregulatory interactions between lymphoid and non-lymphoid cells, protein metabolism regulation, and antigen processing and presentation and affect related pathways, such as the PPAR signaling pathway, AMPK signaling pathway, and GMP-PKG signaling pathway. In the PI3K/Akt pathway, after specific ligands bind to the cell membrane, signals are transmitted through the Akt, JNK and RAS cascades, thus affecting cell proliferation. After PI3K activation, Akt can activate some cyclins and quiescent cells to accelerate the cell cycle and promote the proliferation of ligamentum flavum cells. PPAR α plays a role in the clearance of circulating or cellular lipids by regulating the expression of genes involved in lipid metabolism in liver and skeletal muscle, PPAR β/δ is involved in lipid oxidation and cell proliferation, and the PPAR pathway regulates the expression of genes involved in lipid metabolism, adipogenesis, maintenance of metabolic homeostasis and inflammation. Several published articles confirm that the immune environment of the ligamentum flavum can influence LFH progression. An *in vitro* study determined differential immune scores and immune cell infiltration between OLF and controls and identified and validated 10 OLF-related and immune-related differentially expressed genes (OIDEGs) with different biological function annotations. The lncRNA gene immune cell regulatory network further revealed that 10 OIDEG-related differentially expressed lncRNAs (OIDEs), 41 OIDEs and 7 infiltrating immune cells (OIECs) were highly correlated [39].

To better illustrate these issues, we systematically studied the modification patterns of m6A in the LFH immune microenvironment. The main mechanism of m6A action involves the

recruitment of m6A binding protein (m6A reader) to target RNA. Subsequently, the methyltransferase complex m6A writer within the nuclear spot installs the m6A modification onto the targeted RNA via the methyl group of the S-adenosyl-methionine (SAM) transferase. The expression of most m6A regulators changed between hypertrophic and normal ligamentum flavum, suggesting that m6A regulators play a role in LFH development. The classifier established by the m6A regulator can effectively distinguish healthy and LFH samples, reaffirming the important role of the m6A regulator in disease. Among the 1259 differentially expressed genes, the difference in the readers in the two groups was less than that of Writers and Erasers, and METTL16, PCIF1 and FTO were more important in the prognosis of LFH. In addition, we further constructed a predictive diagnostic model for LFH disease targeting 37 M6A genes (**Figure 7**), and Lasso regression was used to determine the optimal lambda value. The results of the screening revealed that four genes (METTL16, PCIF1, FTO and ALKBH5) could be crucial to the diagnosis of LFH. We also confirmed expression differences between the normal and LFH samples by western blotting. ALKBH5, an important demethylase in OLF development, was found to have increased expression in OLF tissues, which led to the activation of p-Akt, and BMP2 was regulated by ALKBH5 to promote osteogenesis in ligamentum flavum cells [40]. According to Zhang et al., crosstalk between DNMT1 and FTO has been implicated in OLF pathogenesis. FTO has previously been identified as a gene associated with obesity and inflammation, and FTO expression was significantly downregulated in OLF samples, which was positively correlated with SOCS3 expression. In the course of OLF progression, FTO degradation may increase SOCS3 stability and decrease SOCS3 expression in a specific m6A dependent manner [41]. Based on the RT-qPCR results, the expression levels of METTL16, POSTN, TNNC1, MMP1 and PCIF1 were consistent with the results of the bioinformatics analysis. Among these genes, METTL16 has the largest absolute influence coefficient. METTL16 binds the UACAGAGA sequence on the 3'-UTR of MAT2A, a program encoded by SAM synthetase that forms a methylation pattern based on SAM levels. In contrast, the METTL3-METTL14-WTAP complex acts at different levels compared to other indi-

vidual m6A regulators, such as FTO, METTL3 and METTL14. Together, the ALKBH5 expression level influences the prognosis of patients with immune microenvironment of diseases. The METTL16/METTL1 interaction may have important biological implications, including tumor vessel epithelialization, migration, distant metastasis, postoperative fever, and systemic inflammatory response in colorectal cancer (CRC) [42, 43]. Through its N-terminal WW domain, PCIF1 interacts with the phosphorylated CTD of RNA Pol II. Studies of PCIF1-mutated human cells support RNA stabilization of m6A. The conversion of Cap-am mRNA into cap m6Am in human cells mRNA is important for the only necessary and sufficient methyltransferase. Research on its role in disease and immune function remains in its infancy. PCIF1 expression is correlated with ACC, KIRC, KIRP, MESO, THCA OS and DFS, suggesting that PCIF1 has potential application value as a prognostic biomarker in the abovementioned tumors. Jin et al. confirmed that PCIF1 expression is correlated with tumor prognosis and immune invasion, suggesting that PCIF1 may represent a potential target for tumor therapy. Our bioinformatics analysis suggested that PCIF1 might be a potential target for the infiltration of the immune microenvironment of ligamentum flavum hypertrophy [44, 45].

Following that, we calculated the scores for 28 types of immune cells in all samples, conducted clustering, and verified repeatability. The results suggested that the proteins of three genes (ACTA1, MMP1, and TNNC1) can be used as therapeutic targets. Matrix metalloproteinases (MMPs) are a family of metallozinc ion-dependent proteolytic enzymes that are important for the degradation of extracellular matrix (ECM), tissue remodeling, and the regulation of multiple soluble factors within cells. Under normal physiological conditions, MMPs together with tissue inhibitors of metalloproteinases (TIMPs) regulate ECM turnover and maintain cell stability, and MMP dysregulation can accelerate matrix barrier degradation. Poormasjedi Mibod et al. increased the expression of matrix metalloproteinases (MMP1 and MMP3) and inhibited the production of type I collagen and fibronectin by fibroblasts [46]. MMP1 is also involved in the concerted action of proinflammatory cytokines such as IL-6, IL-1, and TNF- α . Synergistically, the production of MMP group

enzymes was inhibited and normal cells were stimulated to produce large amounts of prostaglandin E, while the degree of immune infiltration was controlled [47].

The regulation of the immune environment by POSTN is bidirectional, with some reporting that POSTN promotes the production of inflammatory factors, and it has also been reported that mice deficient in Periostin have higher levels of inflammation, which is possible due to the fact that the low POSTN causes the cells to produce IL-6, IL-8, MMP-1, MMP-3, and MMP-13, all of which may contribute to the development of the disease. POSTN induces cell attachment and spreading and plays a role in cell adhesion, enhancing BMP1 binding in the fibronectin matrix of connective tissue and subsequent proteolytic activation of the lysyl oxidase LOX. Reports have suggested a significant increase in POSTN and α -SMA mRNA levels in the presence of TGF- β in fibroblasts compared with cells from uninvolved skin, and TNF α mRNA levels are significantly lower [48, 49].

Skeletal actin is encoded by ACTA1. A nonregulatory myosin light chain encoded by MYL1 is required for the formation of myofibers. Troponin encoded by TNNC1 is a central regulatory protein of striated muscle contraction. It is involved in the regulation of muscle contraction, skeletal muscle contraction and ventricular myocardial tissue morphogenesis. TNNC1 mutations are associated with familial dilated cardiomyopathy, hypertrophic cardiomyopathy and severe infantile cardiomyopathy [50]. They may be further expressed at high levels in the inflammatory microenvironment to promote ligamentum flavum cell hyperplasia.

Writers and erasers are important for maintaining proper m6A levels and gene expression in human tissues and cells. Our results suggest a positive relationship between METTL3 and CBLL1 and a negative relationship between METTL3 and ZC3H13 as well as ZC3H13 and CBLL1. ZC3H13 is a relevant component of the WMM complex, a complex that mediates m6A methylation of RNA and acts as a key regulator of m6A methylation by promoting m6A methylation of mRNA at 3'-UTRs (by similarity). CBLL1 is a relevant component of the WMM complex, a complex that mediates m6A methylation of RNA. This modification plays a role in the efficiency of mRNA splicing and RNA pro-

cessing. METTL3 heterodimerizes with METTL14 to form an N6 methyltransferase complex that methylates the adenosine residue at position N6 of certain RNAs and regulates various processes, such as the circadian clock, embryonic and hematopoietic stem cell differentiation, cortical neurogenesis, response to DNA damage, T cell differentiation, and primary miRNA processing [51, 52].

Our results indicate that m6A modification provides a new direction for the pathogenesis of immune-related LFH, and m6A modification is involved in the regulation of the LFH immune microenvironment. Epigenetics-related research in the field of LFH is limited. We are the first to explore ligament hypertrophy mechanisms that involve m6A and the immune microenvironment. Combining this information with the latest research on the m6A mechanism and immune microenvironment theory, the pathogenic mechanism of LFH is revealed, emphasizing that epigenetic or RNA modifications are crucial. However, the study has some limitations. First, many of the results were theoretically valid and had some reproducibility in this study based on bioinformatics analysis. Although we validated them at the mRNA level by RT-qPCR and WB, the sample size was small. In addition, how these immune related prediction model genes (METTL16, PCIF1 and FTO) regulate immune infiltration is unclear, and we will further use our target gene prediction website in future studies (<http://rm2target.canceromics.org>). Predictions were made and further validated. The role of HNRNPC in targeting small molecule drugs to inhibit the progress of LFH is also worthy of further exploration. However, all our findings confirm that m6A modification has a powerful impact on LFH immune properties and give us new insights into this disease's pathogenesis.

Conclusion

In summary, this study identified that LFH is caused by coexpression modules of key genes, hub genes, and pathways related to immune responses, inflammation, and cytokines. Systematically evaluating the expression of m6A RNA regulators in LFH and revealing the regulatory mechanisms affecting m6A methylation modification in the LFH immune microenvironment will assist in understanding the intrinsic mechanisms of the LFH immune regulatory net-

Ligamentum flavum hypertrophy on m6A and immune microenvironment

works and in identifying more effective treatments.

Acknowledgements

This work was supported by the National Natural Science Foundation of China (U22A-20162, 82102604, 31900583, 32071351, 81772400), the Natural Science Foundation of Guangzhou City (201807010031), foundation of Shenzhen Committee for Science and Technology Innovation (JCYJ201908091422-11354 GJHZ20180929160004704), Sanming Project of Medicine in Shenzhen (SZSM-201911002), the Beijing Municipal Health Commission (Grant No. BMHC-2021-6, BMHC-2019-9, BMHC-2018-4, PXM2020_026275_000002), AOCMF Translational approaches for bone constructs CPP, Sun Yat-sen University Clinical Research 5010 Program (2019009), and the Academic Affairs Office of Sun Yat-sen University (202211583, 202211589). Special thanks are extended to Cheng Ruijuan for technical support.

Disclosure of conflict of interest

None.

Abbreviations

m6A, N6-methyladenosine; LFH, Ligamentum Flavum Hyperplasia; GEO, Gene Expression Omnibus; GO, Gene Ontology; KEGG, Kyoto Encyclopedia of Genes and Genomes; GSEA, Gene Set Enrichment Analysis; PPI, Protein-Protein Interactions; Lasso, Least absolute shrinkage and selection operator; LF, Ligamentum Flavum; OLF, Ossification of the Ligamentum Flavum; GSVA, Gene Set Variation Analysis; MCODE, Molecular Complex Detection; PCA, Principal Component Analysis; ROC, Receiver Operating Characteristic; DEGs, Differentially Expressed Genes; ssGSEA, single-sample Gene Set Enrichment Analysis.

Address correspondence to: Dr. Xizhe Liu, Guangdong Provincial Key Laboratory of Orthopedics and Traumatology, The First Affiliated Hospital of Sun Yat-sen University, Guangzhou, Guangdong, China. Tel: +86-020-84115962; E-mail: gzxzhliu@qq.com; Dr. Zhiyu Zhou, Innovation Platform of Regeneration and Repair of Spinal Cord and Nerve Injury, Department of Orthopaedic Surgery, The Seventh Affiliated Hospital, Sun Yat-sen University, Shenzhen,

Guangdong, China. Tel: +86-13316942792; E-mail: zhouzhy23@mail.sysu.edu.cn

References

- [1] Sairyo K, Biyani A, Goel V, Leaman D, Booth R Jr, Thomas J, Gehling D, Vishnubhotla L, Long R and Ebraheim N. Pathomechanism of ligamentum flavum hypertrophy: a multidisciplinary investigation based on clinical, biomechanical, histologic, and biologic assessments. *Spine (Phila Pa 1976)* 2005; 30: 2649-2656.
- [2] Hayashi K, Suzuki A, Abdullah Ahmadi S, Terai H, Yamada K, Hoshino M, Toyoda H, Takahashi S, Tamai K, Ohyama S, Javid A, Suhrab Rahmani M, Hasib MM and Nakamura H. Mechanical stress induces elastic fibre disruption and cartilage matrix increase in ligamentum flavum. *Sci Rep* 2017; 7: 13092.
- [3] Sun C, Zhang H, Wang X and Liu X. Ligamentum flavum fibrosis and hypertrophy: molecular pathways, cellular mechanisms, and future directions. *FASEB J* 2020; 34: 9854-9868.
- [4] Nakatani T, Marui T, Hitora T, Doita M, Nishida K and Kurosaka M. Mechanical stretching force promotes collagen synthesis by cultured cells from human ligamentum flavum via transforming growth factor-beta1. *J Orthop Res* 2002; 20: 1380-1386.
- [5] Hu W, Kan S, Liu G, Cao Z and Zhu R. The expression of P16 and S100 associated with elastin degradation and fibrosis of the ligamentum flavum hypertrophy. *BMC Musculoskelet Disord* 2019; 20: 458.
- [6] Sun C, Ma Q, Yin J, Zhang H and Liu X. WISP-1 induced by mechanical stress contributes to fibrosis and hypertrophy of the ligamentum flavum through Hedgehog-Gli1 signaling. *Exp Mol Med* 2021; 53: 1068-1079.
- [7] Sairyo K, Biyani A, Goel VK, Leaman DW, Booth R Jr, Thomas J, Ebraheim NA, Cowgill IA and Mohan SE. Lumbar ligamentum flavum hypertrophy is due to accumulation of inflammation-related scar tissue. *Spine (Phila Pa 1976)* 2007; 32: E340-347.
- [8] Sun C, Tian J, Liu X and Guan G. MiR-21 promotes fibrosis and hypertrophy of ligamentum flavum in lumbar spinal canal stenosis by activating IL-6 expression. *Biochem Biophys Res Commun* 2017; 490: 1106-1111.
- [9] Hayashi K, Suzuki A, Terai H, Ahmadi SA, Rahmani MS, Maruf MH, Habibi H, Hori Y, Yamada K, Hoshino M, Toyoda H, Takahashi S, Tamai K, Ohyama S, Imai Y and Nakamura H. Fibroblast growth factor 9 is upregulated upon intervertebral mechanical stress-induced ligamentum flavum hypertrophy in a rabbit model. *Spine (Phila Pa 1976)* 2019; 44: E1172-E1180.

Ligamentum flavum hypertrophy on m6A and immune microenvironment

- [10] Chuang HC, Tsai KL, Tsai KJ, Tu TY, Shyong YJ, Jou IM, Hsu CC, Shih SS, Liu YF and Lin CL. Oxidative stress mediates age-related hypertrophy of ligamentum flavum by inducing inflammation, fibrosis, and apoptosis through activating Akt and MAPK pathways. *Aging (Albany NY)* 2020; 12: 24168-24183.
- [11] Löhr M, Hampf JA, Lee JY, Ernestus RI, Deckert M and Stenzel W. Hypertrophy of the lumbar ligamentum flavum is associated with inflammation-related TGF- β expression. *Acta Neurochir (Wien)* 2011; 153: 134-141.
- [12] Lu QL, Wang XZ, Xie W, Chen XW, Zhu YL and Li XG. Macrophage migration inhibitory factor may contribute to hypertrophy of lumbar ligamentum flavum in type 2 diabetes mellitus. *Chin Med J (Engl)* 2020; 133: 623-625.
- [13] Nagai S, Hachiya K, Takeda H, Ikeda D, Kawabata S, Watanabe K, Kaneko S and Fujita N. Impact of oxidized LDL/LOX-1 system on ligamentum flavum hypertrophy. *J Orthop Sci* 2022; [Epub ahead of print].
- [14] Jiang X, Liu B, Nie Z, Duan L, Xiong Q, Jin Z, Yang C and Chen Y. The role of m6A modification in the biological functions and diseases. *Signal Transduct Target Ther* 2021; 6: 74.
- [15] Qin Y, Li B, Arumugam S, Lu Q, Mankash SM, Li J, Sun B, Li J, Flavell RA, Li HB and Ouyang X. m(6)A mRNA methylation-directed myeloid cell activation controls progression of NAFLD and obesity. *Cell Rep* 2021; 37: 109968.
- [16] Xie SJ, Lei H, Yang B, Diao LT, Liao JY, He JH, Tao S, Hu YX, Hou YR, Sun YJ, Peng YW, Zhang Q and Xiao ZD. Dynamic m(6)A mRNA methylation reveals the role of METTL3/14-m(6)A-MNK2-ERK signaling axis in skeletal muscle differentiation and regeneration. *Front Cell Dev Biol* 2021; 9: 744171.
- [17] Zuo J, Cao Y, Wang Z, Shah AU, Wang W, Dai C, Chen M, Lin J and Yang Q. The mechanism of antigen-presentation of avian bone marrow dendritic cells suppressed by infectious bronchitis virus. *Genomics* 2021; 113: 1719-1732.
- [18] Nie K, Yi J, Yang Y, Deng M, Yang Y, Wang T, Chen X, Zhang Z and Wang X. A broad m6A modification landscape in inflammatory bowel disease. *Front Cell Dev Biol* 2021; 9: 782636.
- [19] Barrett T, Troup DB, Wilhite SE, Ledoux P, Rudnev D, Evangelista C, Kim IF, Soboleva A, Tomashevsky M and Edgar R. NCBI GEO: mining tens of millions of expression profiles—database and tools update. *Nucleic Acids Res* 2007; 35: D760-765.
- [20] Leek JT, Johnson WE, Parker HS, Jaffe AE and Storey JD. The sva package for removing batch effects and other unwanted variation in high-throughput experiments. *Bioinformatics* 2012; 28: 882-883.
- [21] Ritchie ME, Phipson B, Wu D, Hu Y, Law CW, Shi W and Smyth GK. limma powers differential expression analyses for RNA-sequencing and microarray studies. *Nucleic Acids Res* 2015; 43: e47.
- [22] Yu G, Wang LG, Han Y and He QY. clusterProfiler: an R package for comparing biological themes among gene clusters. *OMICS* 2012; 16: 284-287.
- [23] Subramanian A, Tamayo P, Mootha VK, Mukherjee S, Ebert BL, Gillette MA, Paulovich A, Pomeroy SL, Golub TR, Lander ES and Mesirov JP. Gene set enrichment analysis: a knowledge-based approach for interpreting genome-wide expression profiles. *Proc Natl Acad Sci U S A* 2005; 102: 15545-15550.
- [24] Liberzon A, Birger C, Thorvaldsdóttir H, Ghandi M, Mesirov JP and Tamayo P. The Molecular Signatures Database (MSigDB) hallmark gene set collection. *Cell Syst* 2015; 1: 417-425.
- [25] Hänzelmann S, Castelo R and Guinney J. GSVA: gene set variation analysis for microarray and RNA-seq data. *BMC Bioinformatics* 2013; 14: 7.
- [26] Szklarczyk D, Gable AL, Lyon D, Junge A, Wyder S, Huerta-Cepas J, Simonovic M, Doncheva NT, Morris JH, Bork P, Jensen LJ and Mering CV. STRING v11: protein-protein association networks with increased coverage, supporting functional discovery in genome-wide experimental datasets. *Nucleic Acids Res* 2019; 47: D607-D613.
- [27] Charoentong P, Finotello F, Angelova M, Mayer C, Efremova M, Rieder D, Hackl H and Trajanoski Z. Pan-cancer immunogenomic analyses reveal genotype-immunophenotype relationships and predictors of response to checkpoint blockade. *Cell Rep* 2017; 18: 248-262.
- [28] Steen CB, Liu CL, Alizadeh AA and Newman AM. Profiling cell type abundance and expression in bulk tissues with CIBERSORTx. *Methods Mol Biol* 2020; 2117: 135-157.
- [29] Barretina J, Caponigro G, Stransky N, Venkatesan K, Margolin AA, Kim S, Wilson CJ, Lehár J, Kryukov GV, Sonkin D, Reddy A, Liu M, Murray L, Berger MF, Monahan JE, Morais P, Meltzer J, Korejwa A, Jané-Valbuena J, Mapa FA, Thibault J, Bric-Furlong E, Raman P, Shipway A, Engels IH, Cheng J, Yu GK, Yu J, Aspesi P Jr, de Silva M, Jagtap K, Jones MD, Wang L, Hatton C, Palescandolo E, Gupta S, Mahan S, Sougnez C, Onofrio RC, Liefeld T, MacConaill L, Winckler W, Reich M, Li N, Mesirov JP, Gabriel SB, Getz G, Ardlie K, Chan V, Myer VE, Weber BL, Porter J, Warmuth M, Finan P, Harris JL, Meyerson M, Golub TR, Morrissey MP, Sellers WR, Schlegel R and Garraway LA. Addendum: The Cancer Cell Line Encyclopedia enables predictive modelling of anticancer drug sensitivity. *Nature* 2019; 565: E5-E6.

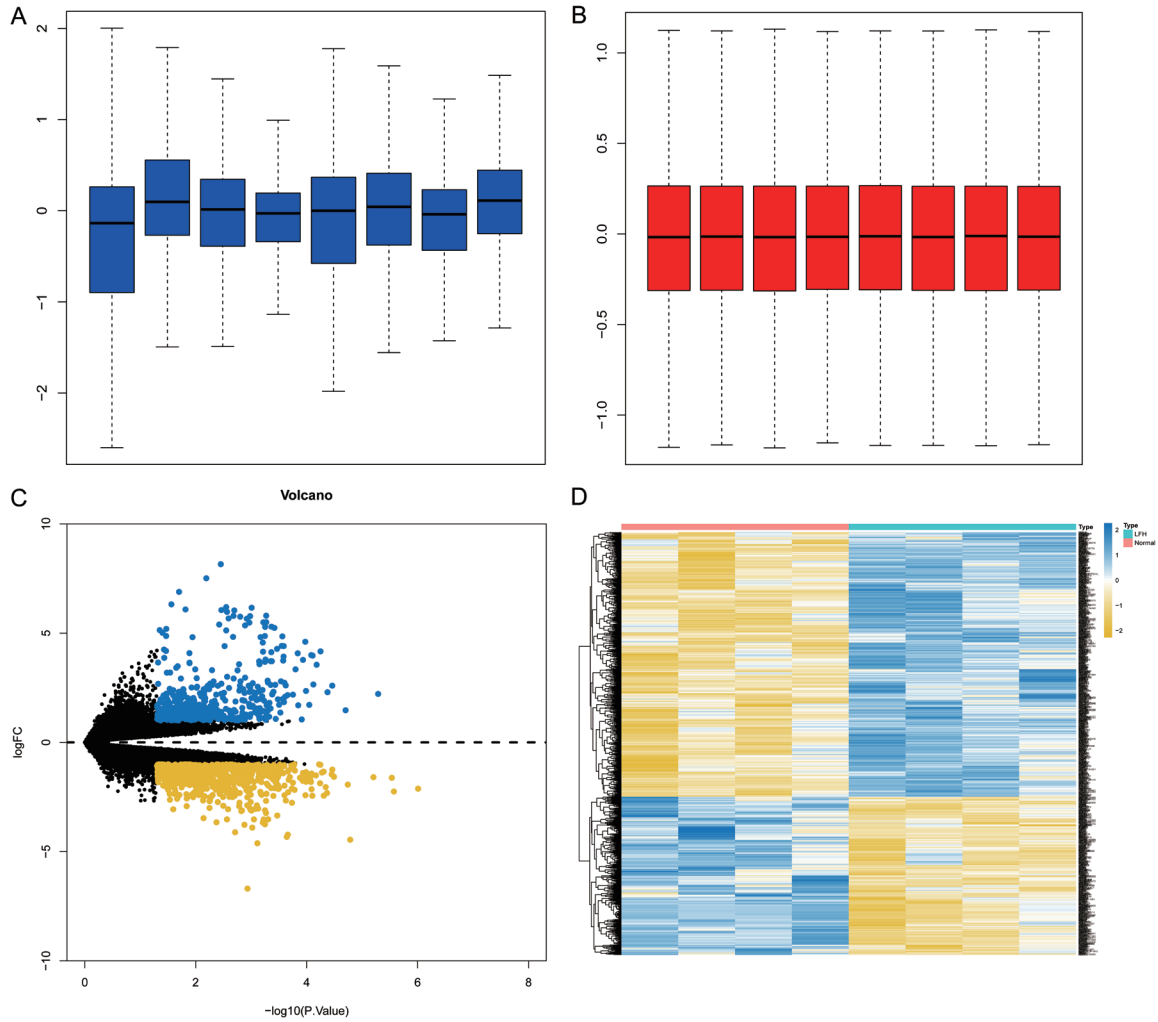
Ligamentum flavum hypertrophy on m6A and immune microenvironment

- [30] Shankavaram UT, Varma S, Kane D, Sunshine M, Chary KK, Reinhold WC, Pommier Y and Weinstein JN. CellMiner: a relational database and query tool for the NCI-60 cancer cell lines. *BMC Genomics* 2009; 10: 277.
- [31] Yang W, Soares J, Greninger P, Edelman EJ, Lightfoot H, Forbes S, Bindal N, Beare D, Smith JA, Thompson IR, Ramaswamy S, Futreal PA, Haber DA, Stratton MR, Benes C, McDermott U and Garnett MJ. Genomics of Drug Sensitivity in Cancer (GDSC): a resource for therapeutic biomarker discovery in cancer cells. *Nucleic Acids Res* 2013; 41: D955-961.
- [32] Dong Q, Li F, Xu Y, Xiao J, Xu Y, Shang D, Zhang C, Yang H, Tian Z, Mi K, Li X and Zhang Y. RNAactDrug: a comprehensive database of RNAs associated with drug sensitivity from multi-omics data. *Brief Bioinform* 2020; 21: 2167-2174.
- [33] Specchia N, Pagnotta A, Gigante A, Logroscino G and Toesca A. Characterization of cultured human ligamentum flavum cells in lumbar spine stenosis. *J Orthop Res* 2001; 19: 294-300.
- [34] Yan B, Huang M, Zeng C, Yao N, Zhang J, Yan B, Jiang H, Tian X, Ao X, Zhao H, Zhou W, Chu J, Wang L, Xian CJ, Zhang Z and Wang L. Locally produced IGF-1 promotes hypertrophy of the ligamentum flavum via the mTORC1 signaling pathway. *Cell Physiol Biochem* 2018; 48: 293-303.
- [35] Livak KJ and Schmittgen TD. Analysis of relative gene expression data using real-time quantitative PCR and the 2(-delta delta C(T)) method. *Methods* 2001; 25: 402-408.
- [36] Nakamura T, Okada T, Endo M, Nakamura T, Oike Y and Mizuta H. Angiopoietin-like protein 2 promotes inflammatory conditions in the ligamentum flavum in the pathogenesis of lumbar spinal canal stenosis by activating interleukin-6 expression. *Eur Spine J* 2015; 24: 2001-2009.
- [37] Saito T, Hara M, Kumamaru H, Kobayakawa K, Yokota K, Kijima K, Yoshizaki S, Harimaya K, Matsumoto Y, Kawaguchi K, Hayashida M, Inagaki Y, Shiba K, Nakashima Y and Okada S. Macrophage infiltration is a causative factor for ligamentum flavum hypertrophy through the activation of collagen production in fibroblasts. *Am J Pathol* 2017; 187: 2831-2840.
- [38] Liu XS, Liu JM, Chen YJ, Li FY, Wu RM, Tan F, Zeng DB, Li W, Zhou H, Gao Y and Pei ZJ. Comprehensive analysis of hexokinase 2 immune infiltrates and m6A related genes in human esophageal carcinoma. *Front Cell Dev Biol* 2021; 9: 715883.
- [39] Zhang B, Chen G, Chen X, Yang X, Fan T, Sun C and Chen Z. Integrating bioinformatic strategies with real-world data to infer distinctive immunocyte infiltration landscape and immunologically relevant transcriptome fingerprints in ossification of ligamentum flavum. *J Inflamm Res* 2021; 14: 3665-3685.
- [40] Wang HF, Kuang MJ, Han SJ, Wang AB, Qiu J, Wang F, Tan BY and Wang DC. BMP2 modified by the m(6)A demethylation enzyme ALKBH5 in the ossification of the ligamentum flavum through the AKT signaling pathway. *Calcif Tissue Int* 2020; 106: 486-493.
- [41] Zhang B, Yuan L, Chen G, Chen X, Yang X, Fan T, Sun C, Fan D and Chen Z. Deciphering obesity-related gene clusters unearths SOCS3 immune infiltrates and 5mC/m6A modifiers in ossification of ligamentum flavum pathogenesis. *Front Endocrinol (Lausanne)* 2022; 13: 861567.
- [42] Ruszkowska A. METTL16, methyltransferase-like protein 16: current insights into structure and function. *Int J Mol Sci* 2021; 22: 2176.
- [43] Zhang B, Gu Y and Jiang G. Expression and prognostic characteristics of m(6) A RNA methylation regulators in breast cancer. *Front Genet* 2020; 11: 604597.
- [44] Joseph J, Kapila YL, Hayami T and Kapila S. Disease-associated extracellular matrix suppresses osteoblastic differentiation of human periodontal ligament cells via MMP-1. *Calcif Tissue Int* 2010; 86: 154-162.
- [45] Akichika S, Hirano S, Shichino Y, Suzuki T, Nishimasu H, Ishitani R, Sugita A, Hirose Y, Iwasaki S, Nureki O and Suzuki T. Cap-specific terminal N (6)-methylation of RNA by an RNA polymerase II-associated methyltransferase. *Science* 2019; 363: eaav0080.
- [46] Jin MZ, Zhang YG, Jin WL and Wang XP. A pan-cancer analysis of the oncogenic and immunogenic role of m6Am methyltransferase PCIF1. *Front Oncol* 2021; 11: 753393.
- [47] Wang T and He C. Pro-inflammatory cytokines: the link between obesity and osteoarthritis. *Cytokine Growth Factor Rev* 2018; 44: 38-50.
- [48] Elliott CG, Forbes TL, Leask A and Hamilton DW. Inflammatory microenvironment and tumor necrosis factor alpha as modulators of periostin and CCN2 expression in human non-healing skin wounds and dermal fibroblasts. *Matrix Biol* 2015; 43: 71-84.
- [49] Sonnenberg-Riethmacher E, Miehle M and Riethmacher D. Periostin in allergy and inflammation. *Front Immunol* 2021; 12: 722170.
- [50] Landstrom AP, Parvatiyar MS, Pinto JR, Marquardt ML, Bos JM, Tester DJ, Ommen SR, Potter JD and Ackerman MJ. Molecular and functional characterization of novel hypertrophic cardiomyopathy susceptibility mutations in TNNC1-encoded troponin C. *J Mol Cell Cardiol* 2008; 45: 281-288.

Ligamentum flavum hypertrophy on m6A and immune microenvironment

- [51] Yue Y, Liu J, Cui X, Cao J, Luo G, Zhang Z, Cheng T, Gao M, Shu X, Ma H, Wang F, Wang X, Shen B, Wang Y, Feng X, He C and Liu J. VIRMA mediates preferential m(6)A mRNA methylation in 3'UTR and near stop codon and associates with alternative polyadenylation. *Cell Discov* 2018; 4: 10.
- [52] Hu C, Yang L, Wang Y, Zhou S, Luo J and Gu Y. Ginsenoside Rh2 reduces m6A RNA methylation in cancer via the KIF26B-SRF positive feedback loop. *J Ginseng Res* 2021; 45: 734-743.

Ligamentum flavum hypertrophy on m6A and immune microenvironment



Supplementary Figure 1. (A) Data set normalization and pre-calibration of the GSE113212 dataset mRNA expression profile matrix box plots; (B) Calibrated GSE113212 dataset mRNA expression profile matrix box plots; Volcano plot (C) and Heatmap (D) of expression differences between the ligamentum flavum hypertrophic samples and normal sample groups in the GSE113212 dataset.

Ligamentum flavum hypertrophy on m6A and immune microenvironment

Supplementary Table 1. Lists the GO enrichment analysis results of DEGs, and the pathways with p.adjust < 0.05 & qvalue < 0.05 were considered significantly enriched, demonstrating the top 10 significantly enriched GO entries

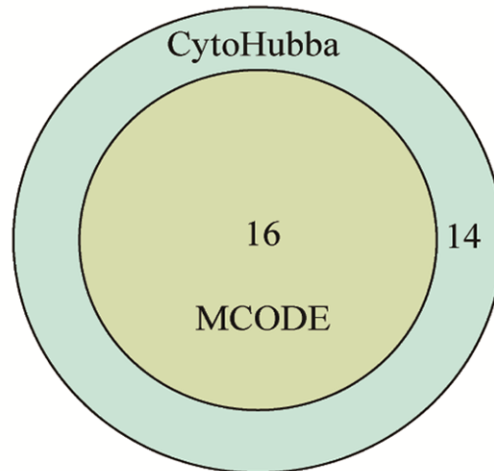
ONTOLOGY	ID	Description	p.adjust	q value	Count
BP	GO:0030198	extracellular matrix organization	4.37E-23	3.50E-23	76
BP	GO:0043062	extracellular structure organization	4.37E-23	3.50E-23	76
BP	GO:0001503	Ossification	2.62E-12	2.10E-12	62
BP	GO:0030199	collagen fibril organization	4.61E-12	3.70E-12	22
BP	GO:0051216	cartilage development	1.98E-08	1.58E-08	37
BP	GO:0061448	connective tissue development	2.66E-07	2.13E-07	41
BP	GO:0002062	chondrocyte differentiation	2.66E-07	2.13E-07	26
BP	GO:0031214	biomineral tissue development	3.35E-07	2.68E-07	30
BP	GO:0110148	Biomineralization	3.35E-07	2.68E-07	30
BP	GO:0006936	muscle contraction	4.51E-07	3.61E-07	48
CC	GO:0062023	collagen-containing extracellular matrix	1.40E-31	1.13E-31	90
CC	GO:0005581	collagen trimer	1.24E-17	1.01E-17	32
CC	GO:0005788	endoplasmic reticulum lumen	3.66E-17	2.96E-17	59
CC	GO:0098644	complex of collagen trimers	9.47E-10	7.67E-10	12
CC	GO:0043202	lysosomal lumen	2.49E-09	2.01E-09	24
CC	GO:0005583	fibrillar collagen trimer	6.32E-09	5.11E-09	9
CC	GO:0098643	banded collagen fibril	6.32E-09	5.11E-09	9
CC	GO:0005775	vacuolar lumen	1.68E-06	1.36E-06	28
CC	GO:0009897	external side of plasma membrane	2.24E-05	1.81E-05	44
CC	GO:0005604	basement membrane	4.20E-05	3.40E-05	18
MF	GO:0005201	extracellular matrix structural constituent	1.23E-21	1.08E-21	49
MF	GO:0030020	extracellular matrix structural constituent conferring tensile strength	1.14E-11	1.00E-11	19
MF	GO:0019838	growth factor binding	1.01E-07	8.87E-08	28
MF	GO:0048018	receptor ligand activity	4.21E-05	3.70E-05	53
MF	GO:0030546	signaling receptor activator activity	4.68E-05	4.11E-05	53
MF	GO:0005125	cytokine activity	5.70E-05	5.01E-05	31
MF	GO:0005539	glycosaminoglycan binding	0.000119	0.000104	31
MF	GO:0005518	collagen binding	0.000139	0.000123	15
MF	GO:0019955	cytokine binding	0.000246	0.000216	21
MF	GO:0030246	carbohydrate binding	0.000402	0.000354	33

Ligamentum flavum hypertrophy on m6A and immune microenvironment

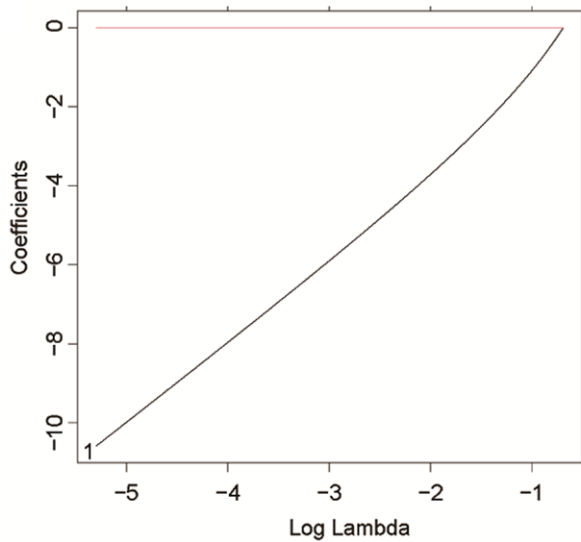
Supplementary Table 2. List of KEGG enrichment analysis results of DEGs. The pathway with p.adjust < 0.05 & qvalue < 0.05 is considered to be significantly enriched, showing all KEGG enrichment entries

ID	Description	p.adjust	q value
hsa05340	Primary immunodeficiency	0.000161	0.000158
hsa04662	B cell receptor signaling pathway	0.000203	0.000198
hsa04640	Hematopoietic cell lineage	0.000652	0.000637
hsa04390	Hippo signaling pathway	0.221697	0.216511
hsa04330	Notch signaling pathway	0.221697	0.216511
hsa05222	Small cell lung cancer	0.221697	0.216511
hsa05225	Hepatocellular carcinoma	0.221697	0.216511
hsa04350	TGF-beta signaling pathway	0.221697	0.216511
hsa04068	FoxO signaling pathway	0.221697	0.216511
hsa05217	Basal cell carcinoma	0.223346	0.218121
hsa04218	Cellular senescence	0.396332	0.387061
hsa00532	Glycosaminoglycan biosynthesis - chondroitin sulfate/dermatan sulfate	0.474559	0.463458
hsa04110	Cell cycle	0.474559	0.463458

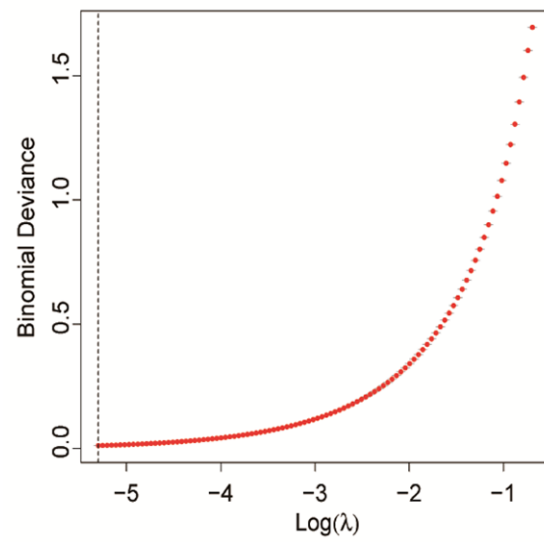
A



B

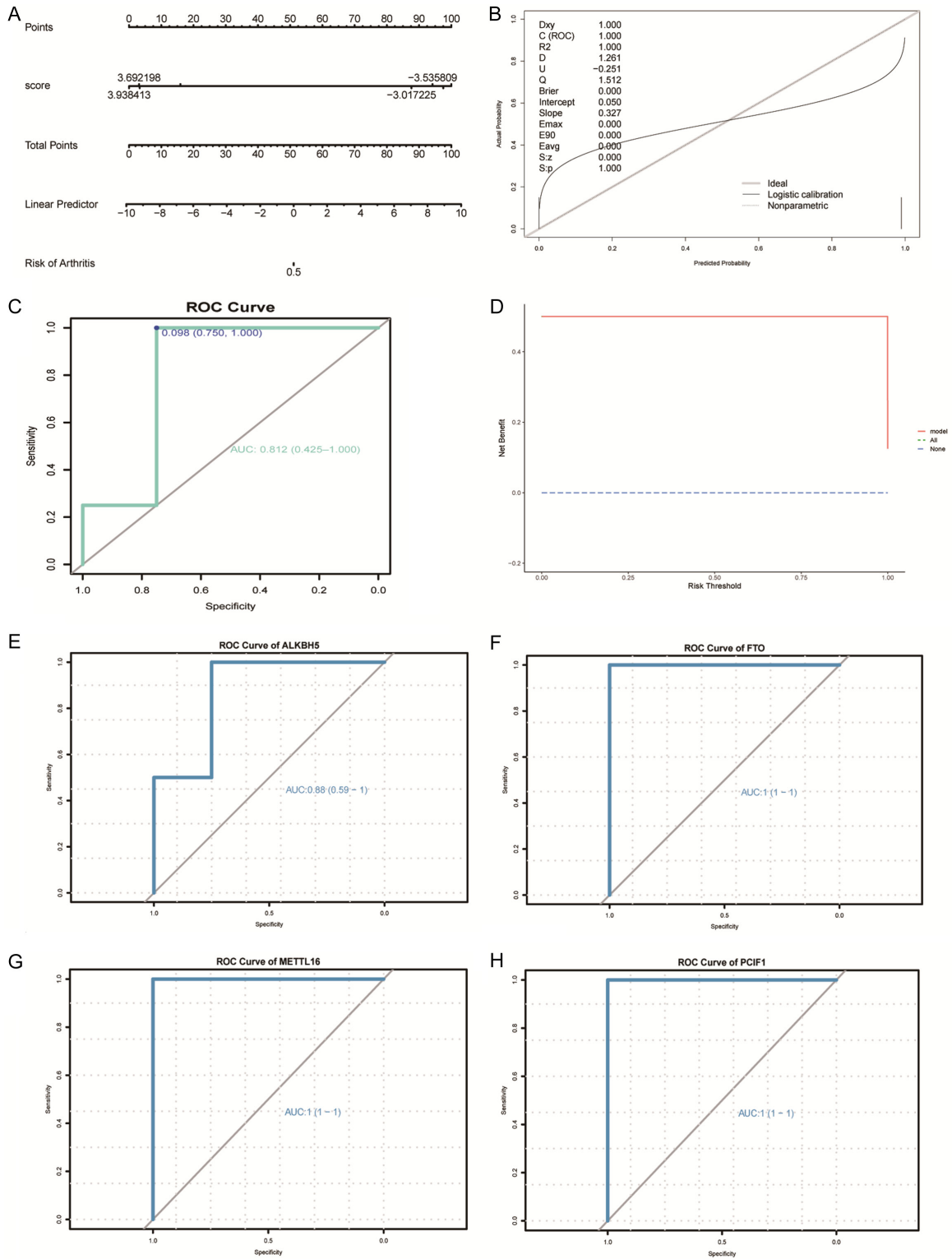


C



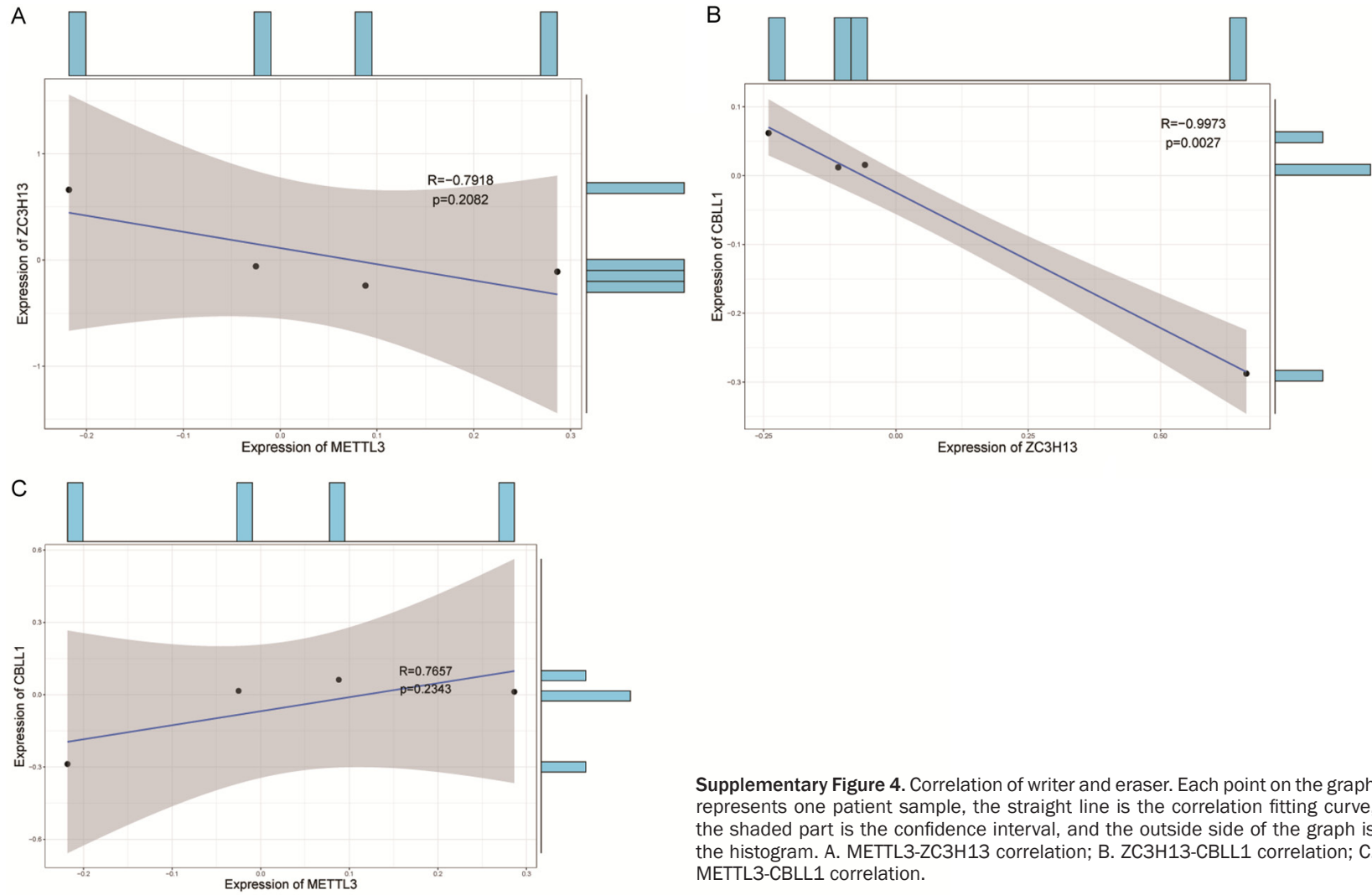
Supplementary Figure 2. (A) Intersection of significant nodes from CytoHubba and MCODE screening to obtain 16 hub genes; (B, C) Construction of an LFH immune related diagnostic model based on the hub genes. Regression screening was first performed using the lasso method, and the optimal lambda value lasso regression curve was determined. Results demonstrate the convergent screening process of lasso regression for 16 gene features, with the x-axis as the log lambda value and the y-axis as the regression coefficient (B); Lambda value selection curves were used to select the optimal lambda value for the lasso regression model, typically by picking the lowest point, which is the optimal lambda value at the dotted left-hand side of the plot (C).

Ligamentum flavum hypertrophy on m6A and immune microenvironment



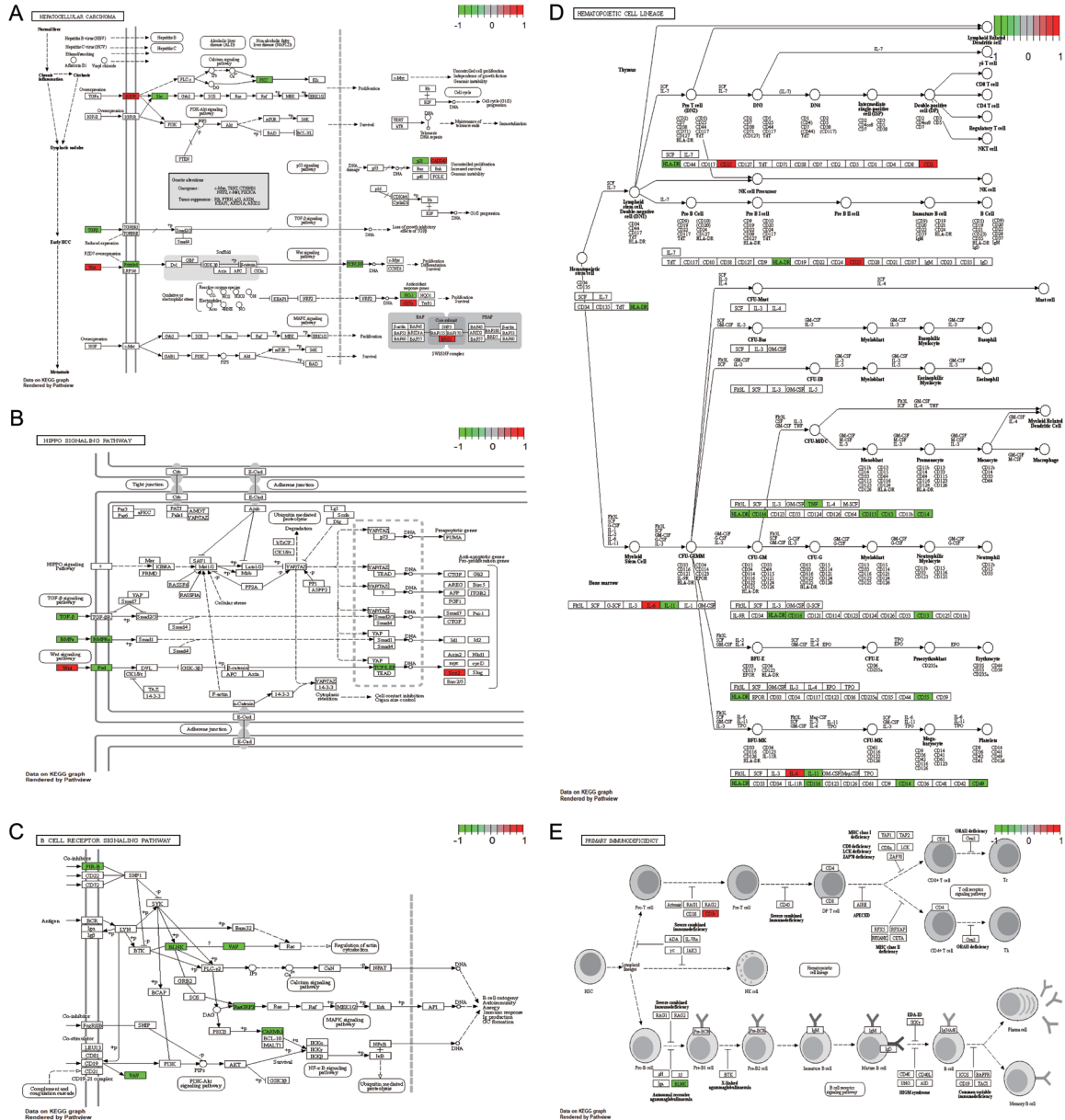
Supplementary Figure 3. Validation of m6A genetic diagnostic model. A. Nomogram with predictors on the left and bars on the right; B. Recall curve. Emax is the maximum offset of the model from the ideal, and Eavg is the minimum offset of the model from the ideal. S: P, when S: P > 0.05 stated beyond the calibration test. C (ROC) is the area under the ROC curve; C. Overall ROC curve for the 4 genes. The x-axis is specificity, Y-axis is sensitivity, and AUC is area under the curve; D. DAC curves. The x-axis is the risk threshold, the y-axis is the net benefit rate, the blue dotted line represents the 0 net benefit rate, all (green dotted line) represents all samples received intervention, and model (red solid line) represents the model curve; E-H. Single gene ROC curves for the 4 genes, respectively, which exemplifies the superior diagnostic efficacy.

Ligamentum flavum hypertrophy on m6A and immune microenvironment



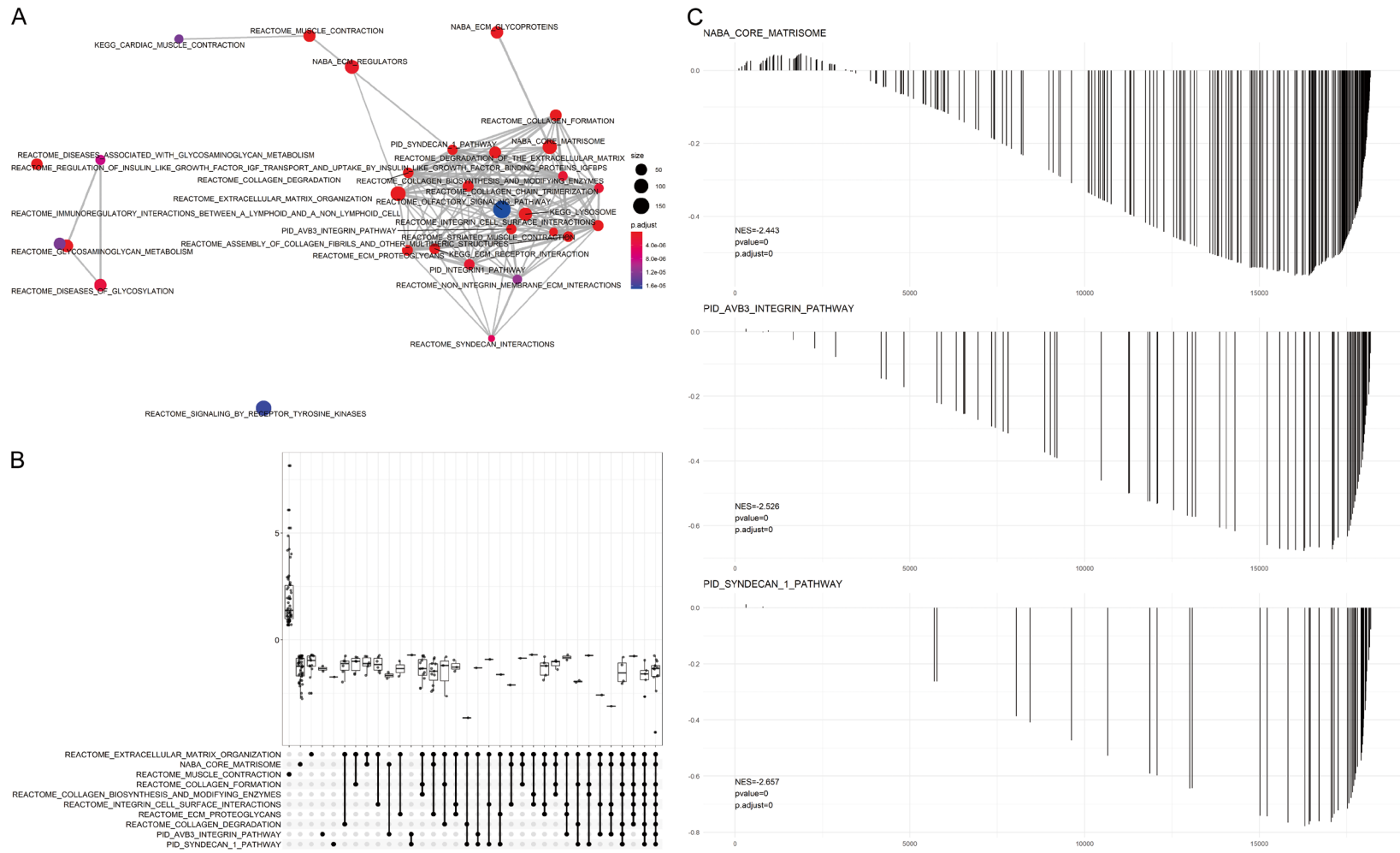
Supplementary Figure 4. Correlation of writer and eraser. Each point on the graph represents one patient sample, the straight line is the correlation fitting curve, the shaded part is the confidence interval, and the outside side of the graph is the histogram. A. METTL3-ZC3H13 correlation; B. ZC3H13-CBLL1 correlation; C. METTL3-CBLL1 correlation.

Ligamentum flavum hypertrophy on m6A and immune microenvironment



Supplementary Figure 5. KEGG enrichment analysis of DEGs between the hypertrophy and normal sample groups of ligamentum flavum is shown in (A-E) Enriched KEGG signaling pathways, with red representing upregulated enriched genes in the pathway and green representing downregulated enriched genes in the pathway. Hepatocellular carcinoma (A); Hippo signaling pathway (B); B cell receptor signaling pathway (C); Hematopoietic cell lineage (D); Primary immunodeficiency (E). KEGG: Kyoto Encyclopedia of Genes and Genomes.

Ligamentum flavum hypertrophy on m6A and immune microenvironment



Supplementary Figure 6. A-C. Molecular characteristic network diagram, upset diagram and GSEA enrichment diagram of GSEA enrichment analysis.

Ligamentum flavum hypertrophy on m6A and immune microenvironment

Supplementary Table 3. List of GSEA enrichment analysis results, including enrichment entries with $|NSE| > 2$

ID	Description	enrichment Score	NES	p.adjust	qvalues
BP	GO:0001501	-0.4789	-2.22241	0.016287	0.01074
BP	GO:0001503	-0.45125	-2.0326	0.016287	0.01074
BP	GO:0030198	-0.55712	-2.50369	0.016287	0.01074
BP	GO:0043062	-0.55682	-2.50044	0.016287	0.01074
BP	GO:0060348	-0.51035	-2.15915	0.016287	0.01074
BP	GO:0051216	-0.51849	-2.17626	0.016287	0.01074
BP	GO:0042476	-0.50455	-2.00715	0.016287	0.01074
BP	GO:0030203	-0.51888	-2.10604	0.016287	0.01074
BP	GO:0006024	-0.5858	-2.26355	0.016287	0.01074
BP	GO:1903510	-0.54478	-2.10792	0.016287	0.01074
CC	GO:0062023	-0.50516	-2.29404	0.016287	0.01074
CC	GO:0005788	-0.5308	-2.33201	0.016287	0.01074
CC	GO:0022626	0.529688	2.075623	0.016287	0.01074
CC	GO:0030018	0.693471	2.76785	0.016287	0.01074
CC	GO:0043292	0.708866	3.055294	0.016287	0.01074
CC	GO:0031674	0.698084	2.809029	0.016287	0.01074
CC	GO:0030016	0.713433	3.042546	0.016287	0.01074
CC	GO:0030017	0.732185	3.083101	0.016287	0.01074
CC	GO:0015629	0.449201	2.078963	0.016547	0.010912
MF	GO:0005201	-0.60528	-2.45564	0.016287	0.01074
MF	GO:0051015	0.484924	2.023892	0.016287	0.01074
MF	GO:0003779	0.46185	2.122282	0.016287	0.01074
hsa04260	Cardiac muscle contraction	0.626079	2.293335	0.025588	0.019285
hsa05152	Tuberculosis	-0.48782	-2.00297	0.025588	0.019285
hsa00532	Glycosaminoglycan biosynthesis - chondroitin sulfate/dermatan sulfate	-0.73594	-2.03594	0.025588	0.019285
hsa04512	ECM-receptor interaction	-0.55976	-2.06289	0.025588	0.019285
hsa04974	Protein digestion and absorption	-0.5594	-2.10935	0.025588	0.019285
hsa04612	Antigen processing and presentation	-0.5955	-2.11821	0.025588	0.019285
hsa04380	Osteoclast differentiation	-0.54132	-2.12787	0.025588	0.019285
hsa04145	Phagosome	-0.54918	-2.19667	0.025588	0.019285
hsa05323	Rheumatoid arthritis	-0.5983	-2.20494	0.025588	0.019285
hsa04142	Lysosome	-0.57908	-2.27629	0.025588	0.019285

Ligamentum flavum hypertrophy on m6A and immune microenvironment

Supplementary Table 4. List of GSEA enrichment analysis msigdb results, including enrichment entries with $|NSE| > 2$

ID	Enrichment Score	NES	p.adjust	q values
NABA_CORE_MATRISOME	-0.56563	-2.44345	1.47E-08	1.30E-08
PID_AVB3_INTEGRIN_PATHWAY	-0.68924	-2.52614	1.47E-08	1.30E-08
PID_SYNDECAN_1_PATHWAY	-0.79154	-2.6566	1.47E-08	1.30E-08
REACTOME_COLLAGEN_BIOSYNTHESIS_AND_MODIFYING_ENZYMES	-0.72031	-2.531	1.47E-08	1.30E-08
REACTOME_COLLAGEN_DEGRADATION	-0.70252	-2.46849	1.47E-08	1.30E-08
REACTOME_COLLAGEN_FORMATION	-0.71807	-2.68654	1.47E-08	1.30E-08
REACTOME_ECM_PROTEOGLYCANS	-0.67694	-2.47529	1.47E-08	1.30E-08
REACTOME_EXTRACELLULAR_MATRIX_ORGANIZATION	-0.5657	-2.48143	1.47E-08	1.30E-08
REACTOME_INTEGRIN_CELL_SURFACE_INTERACTIONS	-0.63859	-2.3977	1.47E-08	1.30E-08
REACTOME_MUSCLE_CONTRACTION	0.576806	2.451098	1.47E-08	1.30E-08
REACTOME_REGULATION_OF_INSULIN_LIKE_GROWTH_FACTOR_IGF_TRANSPORT_AND_UPTAKE_BY_INSULIN_LIKE_GROWTH_FACTOR_BINDING_PROTEINS_IGFBPS	-0.59442	-2.33643	1.47E-08	1.30E-08
REACTOME_STRIATED_MUSCLE_CONTRACTION	0.85692	2.694424	1.47E-08	1.30E-08
REACTOME_DEGRADATION_OF_THE_EXTRACELLULAR_MATRIX	-0.56582	-2.25344	1.47E-08	1.30E-08
KEGG_LYSOSOME	-0.58713	-2.28933	3.65E-08	3.21E-08
REACTOME_ASSEMBLY_OF_COLLAGEN_FIBRILS_AND_OTHER_MULTIMERIC_STRUCTURES	-0.70366	-2.46913	3.65E-08	3.21E-08
KEGG_ECM_RECEPTOR_INTERACTION	-0.62689	-2.34558	8.89E-08	7.82E-08
NABA_ECM_GLYCOPROTEINS	-0.50184	-2.078	4.16E-07	3.66E-07
REACTOME_GLYCOSAMINOGLYCAN_METABOLISM	-0.56262	-2.21475	4.87E-07	4.29E-07
PID_INTEGRIN1_PATHWAY	-0.6508	-2.33521	1.77E-06	1.55E-06
NABA_COLLAGENS	-0.69721	-2.288	2.00E-06	1.76E-06
REACTOME_COLLAGEN_CHAIN_TRIMERIZATION	-0.69721	-2.288	2.00E-06	1.76E-06
REACTOME_DISEASES_OF_GLYCOSYLATION	-0.51546	-2.06022	2.94E-06	2.59E-06
REACTOME_SYNDECAN_INTERACTIONS	-0.78562	-2.35609	5.11E-06	4.49E-06
REACTOME_DISEASES_ASSOCIATED_WITH_GLYCOSAMINOGLYCAN_METABOLISM	-0.70329	-2.29023	8.29E-06	7.29E-06
REACTOME_NON_INTEGRIN_MEMBRANE_ECM_INTERACTIONS	-0.64617	-2.2674	1.11E-05	9.81E-06
REACTOME_IMMUNOREGULATORY_INTERACTIONS_BETWEEN_A_LYMPHOID_AND_A_NON_LYMPHOID_CELL	-0.53023	-2.08725	1.28E-05	1.13E-05
KEGG_CARDIAC_MUSCLE_CONTRACTION	0.622575	2.25698	1.30E-05	1.14E-05
REACTOME_MET_ACTIVATES_PTK2_SIGNALING	-0.7408	-2.29102	2.46E-05	2.16E-05
KEGG_LEISHMANIA_INFECTION	-0.59712	-2.17884	4.62E-05	4.07E-05
REACTOME_CHONDROITIN_SULFATE_DERMATAN_SULFATE_METABOLISM	-0.63566	-2.15663	9.28E-05	8.16E-05
REACTOME_MET_PROMOTES_CELL_MOTILITY	-0.65602	-2.1363	0.000292	0.000257

Ligamentum flavum hypertrophy on m6A and immune microenvironment

PID_INTEGRIN3_PATHWAY	-0.64324	-2.09772	0.000489	0.00043
KEGG_ANTIGEN_PROCESSING_AND_PRESENTATION	-0.54396	-2.00202	0.000602	0.00053
REACTOME_GLYCOPHINGOLIPID_METABOLISM	-0.61626	-2.02237	0.000748	0.000658
REACTOME_SIGNALING_BY_PDGF	-0.5768	-2.02358	0.000799	0.000703
KEGG_GLYCOSAMINOGLYCAN_BIOSYNTHESIS_CHONDROITIN_SULFATE	-0.74055	-2.12034	0.00087	0.000766
KEGG_RIBOSOME	0.541545	2.010157	0.001028	0.000904
REACTOME_TRAFFICKING_AND_PROCESSING_OF_ENDOSOMAL_TLR	-0.86493	-2.07798	0.001028	0.000904
REACTOME_FATTY_ACIDS	0.827626	2.098822	0.001342	0.001181
REACTOME_NONSENSE_MEDIATED_DECAY_NMD_INDEPENDENT_OF_THE_EXON_JUNCTION_COMPLEX_EJC	0.52893	2.00445	0.001342	0.001181
NABA_PROTEOGLYCANS	-0.65011	-2.06641	0.00135	0.001188
PID_SYNDECAN_4_PATHWAY	-0.66744	-2.07504	0.001533	0.001348
PID_INTEGRIN_A9B1_PATHWAY	-0.7043	-2.06271	0.001623	0.001428
REACTOME_TRIGLYCERIDE_METABOLISM	0.664653	2.106625	0.00168	0.001478
KEGG_HYPERTROPHIC_CARDIOMYOPATHY_HCM	0.545223	2.000558	0.00168	0.001478
REACTOME_SCAVENGING_BY_CLASS_A_RECEPTORS	-0.7539	-2.09775	0.00213	0.001874
REACTOME_KERATAN_SULFATE_KERATIN_METABOLISM	-0.6435	-2.01092	0.003712	0.003266
BIOCARTA_MHC_PATHWAY	-0.7808	-2.0102	0.009085	0.007993